Quaternary International 542 (2020) 65–79

Contents lists available at ScienceDirect

Quaternary International

journal homepage: www.elsevier.com/locate/quaint

Revisiting the chronostratigraphy of Late Pleistocene loess-paleosol sequences in southwestern Ukraine: OSL dating of Kurortne section

Viorica Tecsa[a,b], Natalia Gerasimenko[c], Daniel Veres[d,a,*], Ulrich Hambach[e], Frank Lehmkuhl[f], Philipp Schulte[f], Alida Timar-Gabor[a,b]

[a] Interdisciplinary Research Institute on Bio-Nano-Sciences, Babeș-Bolyai University, Cluj-Napoca, Romania
[b] Faculty of Environmental Sciences and Engineering, Babeș-Bolyai University, Cluj-Napoca, Romania
[c] Taras Shevshenko National University, Kiev, Ukraine
[d] Romanian Academy, Institute of Speleology, Cluj-Napoca, Romania
[e] BayCEER & Chair of Geomorphology, University of Bayreuth, Germany
[f] Department of Geography, RWTH Aachen University, Aachen, Germany

ARTICLE INFO

Keywords:
Loess chronostratigraphy
OSL dating
Last glacial cycle
SE Europe
Ukraine

ABSTRACT

Due to the general lack of other high-resolution paleoclimate records, loess-paleosol sequences are crucial archives for disentangling past climate variability in southeastern Europe. Here we present results of a multi proxy sedimentological and geochemical investigation of Kurortne loess-paleosol section from southwestern Ukraine, coupled with detailed optically stimulated luminescence (OSL) dating. OSL investigations were carried out on quartz grains of different grain sizes (4–11 μm, 63–90 μm and 90–125 μm), using the single aliquot regenerative (SAR) protocol. The OSL dating results are in line with previous findings on dating loess-paleosol sequences along the Black Sea shore in Romania, as well as worldwide: (i) ages obtained on different grain sizes are in agreement for equivalent doses of less than 200 Gy, whereas for higher equivalent doses 4–11 μm ages underestimate the coarser fraction ages; and (ii) an inverse correlation between dated grain size fractions and saturation characteristics is reported.

Our combined dating and sedimentological approach would confirm that the investigated uppermost 4.5 m at Kurortne cover the Last Glacial Cycle, adding important data in better constraining local and regional chronostratigraphic correlations. The application of the SAR protocol on 63–90 μm quartz grains on samples collected from the lower part of S1 soil (the Kaydaky unit) and from the Kaydaky/Pryluky units boundary produced ages of 123 ± 10 ka and 85 ± 6 ka, respectively. As the temporal range covered by these units in the Ukrainian Quaternary stratigraphic framework is still debatable, our results confirm the broad correlation of the Kaydaky-Pryluky paleosol units at Kurortne with the last interglacial (i.e., MIS 5). Dating the Uday and Bug loess units produced ages corresponding to MIS 4 and MIS 2, respectively, whereas the sample collected from the Vytachiv unit provided an age of 37.7 ± 2.4 ka, assigning this paleosol to MIS 3. On the basis of trends in the magnetic enhancement, the onset of pedogenetic processes likely commenced already around 20 ka, but the formation of the topmost S0 soil has begun after 13.8 ± 1.0 ka.

1. Introduction

Loess-paleosol sequences (LPS) in Europe are important paleoclimate archives for recording the long-term environmental history of terrestrial landscapes (Frechen et al., 2003; Marković et al., 2015; Rousseau et al., 2017). The size of the loess fields commencing in the Middle and Lower Danube basins and extending to the Russian Plain (Haase et al., 2007) would roughly equal that of the Chinese Loess Plateau (CPL). This fact and the lack of other long-term paleoclimate records renders the Ukrainian LPS (Fig. 1) as valuable archives for disentangling Quaternary paleoclimate evolution in the northern Black Sea area (Veklitch, 1982, 1993; Sirenko and Turlo, 1986; Velichko, 1990; Gozhik et al., 1995, 2000, 2013; Lindner et al., 2004, 2006; Gerasimenko, 2006, 2011; Bolikhovskaya and Molodkov, 2006; Matviishina et al., 2010; Boguckyj et al., 2013), and a link between west European (Rousseau et al., 2011; Marković et al., 2015; Sümegi et al., 2019) and Central Asian loess paleoclimate records (Zeeden et al., 2018a; Fitzsimmons, 2017).

* Corresponding author. Interdisciplinary Research Institute on Bio-Nano-Sciences, Babeș-Bolyai University, Cluj-Napoca, Romania.
E-mail address: daniel.veres@ubbcluj.ro (D. Veres).

https://doi.org/10.1016/j.quaint.2020.03.001
Received 27 September 2019; Received in revised form 1 March 2020; Accepted 2 March 2020
Available online 05 March 2020

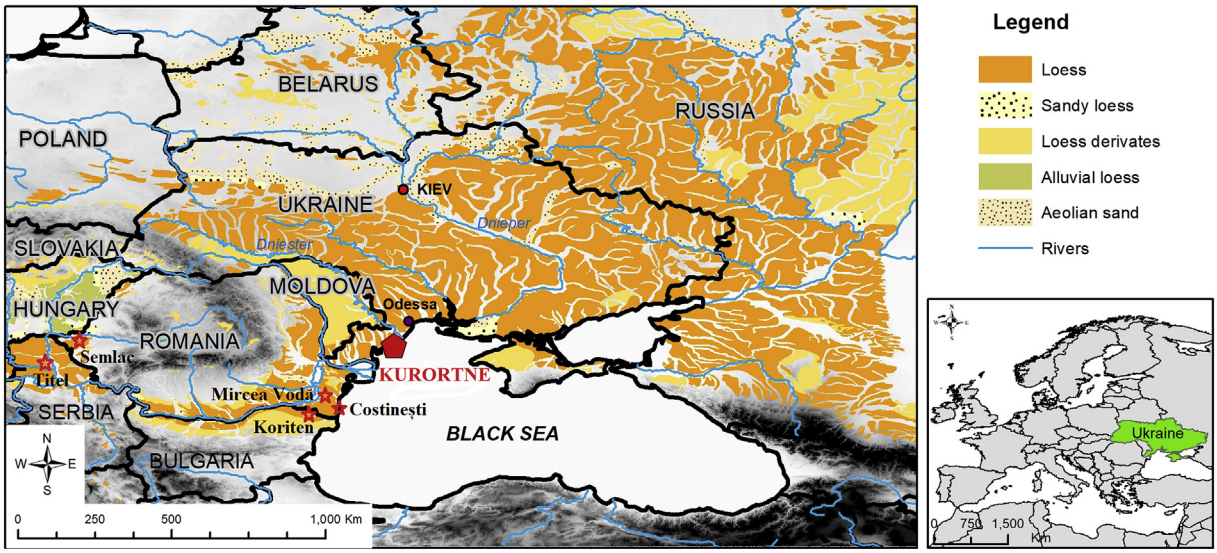

Fig. 1. Location of the studied Kurortne loess-paleosol sequence in southwestern Ukraine, alongside the distribution of loess and loess-derivate deposits in southeastern and eastern Europe after Hasse et al. (2007). Other loess-paleosol sequences discussed in the main text are also indicated.

Albeit significant recent progress in loess paleoclimatology (see review in Schaetzl et al., 2018), more reliable comparisons between LPS and marine or ice-core records are needed (Zeeden et al., 2018a,b; Marković et al., 2018; Újvári et al., 2018; Sümegi et al., 2019) for deeper understanding of past climate change and for better assessing the role of loess-paleosol proxies in reconstructing regional paleoclimate dynamics (Maher et al., 2010; Hao et al., 2012; Constantin et al., 2019; Obreht et al., 2019).

In this respect, local national stratigraphic considerations based on phenomenological appearance of sedimentary and/or pedological units, and often lacking up-to-date paleoclimatic data and reliable chronological control preclude achieving a uniform approach on comparisons with, for example Marine Isotope Stages (MIS), as proposed for both western European (Rousseau et al., 2017) and the Danube Basin loess records (Marković et al., 2015, 2018). The unified Danube Basin loess framework (Marković et al., 2015) is important for securely correlating different national nomenclatures as it allowed for better integration of long-term trends in loess paleoclimate proxies for both, the Danube loess records on one hand, and to the CPL loess records on the other hand (see Zeeden et al., 2018a).

For the Last Glacial Cycle (LGC), the Ukrainian Quaternary stratigraphic framework (Veklitch, 1993) above the Dnipro unit (dn, previously spelled Dnieper), which presumably includes the Saalian (thus MIS 6) glacial deposits in northern Ukraine, but mainly loess and loess-derivates in southern Ukraine, consists of eight main stratigraphic units as following (from bottom): the Kaydaky (kd) soil, Tyasmyn (ts) loess, Pryluky (pl) soil, Uday (ud) loess, Vytachiv (vt) soil, Bug (bg) loess, Dofinivka (df) soil and Prychornomorya (pč) loess. The Prychornomorya unit is subdivided into two loess subunits (the lower 'pc_1' and the upper 'pc_3') separated by subunit (pc_2) which includes incipient soils. The Prychornomorya, Dofinivka, and Bug units are generally considered of MIS 2 age, whereas Vytachiv and Uday units are regarded as correlatives of MIS 3 and MIS 4, respectively. The correlation of units within the lower part of the Ukrainian chronostratigraphic framework is still debated. Some authors correlate the Dnipro, Kaydaky, Tyasmyn and Pryluky units with MIS 8, MIS 7, MIS 6, and MIS 5, respectively (Veklitch, 1993; Gozhik et al., 2000, 2014; Boguckyj and Lanczont, 2002; Lindner et al., 2004, 2006; Boguckyj et al., 2013). On the other hand, in several studies the Dnipro unit was correlated with MIS 6, whereas the Kaydaky, Tyasmyn, and Pryluky units were linked to MIS 5e, 5d, and 5c-a, respectively (Rousseau et al., 2001, 2011; Vozgrin, 2001; Gerasimenko, 2004, 2006; Buggle et al., 2008, 2009; Matviishina et al., 2010; Bokhorst et al., 2011; Haesaerts et al., 2016).

In light of such chronostratigraphic issues, better resolved loess chronologies (e.g., Újvári et al., 2017; Moine et al., 2017) appear crucial for developing reliable regional stratigraphic models (Marković et al., 2015; Zeeden et al., 2018a), with luminescence dating providing the potential for testing and refining correlations (Stevens et al., 2018; Veres et al., 2018; Perić et al., 2019; Constantin et al., 2019). In order to compare the Ukrainian loess-paleosol chronostratigraphic scheme to the unified stratigraphic model of the southeastern European loess records (Marković et al., 2015), we focus here on the uppermost 4.5 m of the Kurortne LPS (southwestern Ukraine; Fig. 1) that in our view extends over the LGC. It shall be noted that Gozhik et al. (1995, 2000) investigated the Kurortne LPS in accordance with the stratigraphy of the neighboring section Prymorskoje (as defined by Veklitch et al., 1967), and the Kurortne section itself has also been reported as Prymorskoje in some papers (Gozhik et al., 1995; Nawrocki et al., 1999). In these previous works, the uppermost loess unit capped by the Holocene soil was related to the Prychornomorya unit, the underlying two uppermost paleosols were regarded as the Dofinivka pedocomplex, and the underlying thick loess related to the Bug unit. Thus, following these authors, the part of the section studied here (i.e., uppermost 4.5 m) relates mainly to MIS 2. The pedocomplex underlying the Bug unit was consequently regarded as equivalent of MIS 3. This chronostratigraphic framework was supported by debatable radiocarbon dates on bulk organic matter, with the uppermost loess unit dated to 12.6 ± 0.25 ^{14}C uncalibrated (^{14}C) ka BP, the second paleosol yielded an age of 16.3 ± 0.30 ^{14}C ka BP, and the thick loess below was dated to 21.3 ± 0.30 ^{14}C ka BP and 26.1 ± 0.39 ^{14}C ka BP, respectively (Gozhik et al., 1995, 2000).

On the contrary, detailed studies of LPS along a submeridional transect throughout Ukraine (Vozgrin, 2001, 2005; Veklitch, 2018) suggest that adjacent to the Black Sea shoreline, the Prychornomorya and Bug loess units are mainly very thin, the upper two paleosols by their pedomorphological characteristics most likely belong to the Vytachiv, Pryluky, and Kaydaky units (rather than to the Dofinivka pedocomplex), the latter two often welded and not separated by Tyasmyn loess unit as also seen in other profiles throughout Ukraine (Veklitch, 1982; Gerasimenko, 2006; Matviishina et al., 2010). Furthermore, the second thickest loess unit from top to bottom should relate to the Dnipro unit and not to the Bug loess (as suggested by Gozhik et al., 1995, 2000; Boguckyj et al., 2013).

Such local chronostratigraphic issues that apply also to other loess

sites in southwestern Ukraine, including Roxolany (see contradictory chronostratigraphic implications discussed in Gožik et al., 1976; Tsatskin et al., 1998; Dodonov et al., 2006; Gendler et al., 2006; Boguckyj et al., 2013; Bakhmutov et al., 2017; Nawrocki et al., 2018) impact upon the potential integration of Ukrainian loess data into a pan-European loess stratigraphic model (Marković et al., 2015, 2018). This is even more compelling when such records are employed in regional correlations schemes (Necula et al., 2015; Marković et al., 2018) with limited direct chronological control for different records.

Here we discuss Late Pleistocene environmental dynamics in southwestern Ukraine based on integrating optically stimulated luminescence (OSL) dating of quartz of different grain sizes (4–11 μm, 63–90 μm and 90–125 μm), with high-resolution rock magnetic data, grain size and geochemical proxies for Kurortne LPS. Through comparison with other records from the Danube – Black Sea loess fields we show that the investigated sequence extends over the LGC, providing an important link to other regional LPS, and a key record for comparison of the Ukrainian Quaternary stratigraphy with the Danube loess model (Marković et al., 2015).

2. Study site

The Kurortne LPS (45°54′ N, 30°16′ E) is located near Kurortne village (Odessa region, Ukraine), at the Black Sea shore (Fig. 1). The section comprises ca. 15 m of intercalated loess and paleosol units (Gozhik et al., 2000), and for this study we have investigated in detail the uppermost 4.5 m (Figs. 2–3). In order to augment the existing chronostratigraphic framework for Kurortne LPS, 12 samples for optically stimulated luminescence (OSL) dating were collected in 15-cm long metal tubes. For sedimentological and geochemical analyses samples were collected contiguously at 2 cm resolution down to 130 cm depth, whereas to the depth of 450 cm sampling was carried out at 4 cm resolution. For ease of establishing a reliable regional comparison to the neighboring Danube loess stratigraphic concept, we follow also the approach of Marković et al. (2015) in defining paleosol and loess units, alongside the Ukrainian Quaternary stratigraphic nomenclature (Veklitch, 1993). From top to bottom the investigated sequence at Kurortne comprises the following:

The *Holocene (hl) soil* (or S0 following Marković et al., 2015) is a chernozem of the subtype 'common', around 1 m thick clearly separated into three genetic horizons (Figs. 2–3). The uppermost A1 horizon is dark grey (almost black), silty, carbonate poor, loose and porous, with a granular structure and a gradual transition downwards. The A1B horizon is dark brownish-grey, silty, more compacted than the A1 horizon, and with larger granular structure. Carbonates became abundant from 40 cm depth (diffused carbonate mantle on root channels below 50 cm depth). The lower boundary is gradual. The Ck horizon is pale yellowish-brown loess-like silt, strongly enriched in carbonates (below 65 cm), with very weak prismatic structure, without clay coatings. Small and soft carbonate nodules occur from 75 cm depth, and carbonate nodules form rhyzolithes below 80 cm depth. The horizon preserves many krotovinas and root channels filled with humus, and the matrix of the Ck horizon indicates that it most likely comprises material of the Prychornomorya loess unit (between 0.7 and 1.0 m depth). Seven luminescence samples (PRI-1.1 to 1.7) were collected from the Holocene soil and the transitional horizon Ck to the underlying loess unit (Figs. 2–3).

The *Bug (bg) loess unit* (1.00–1.35 m) or the L1LL1 (Marković et al., 2015) comprises a thin loess bed made up of light brown-yellowish silt, slightly pedogenetically overprinted, preserving also rhyzolithes and soft carbonate nodules. The lower boundary is well visible and OSL sample PRI-1.8 was collected from the middle part of this unit (Figs. 2–3).

The *Vytachiv (vt) paleosol unit* (or L1SS1) extends between 1.35 and 2.00 m and comprises two genetic horizons. The A1k horizon is brown, with weak prismatic structure, slightly compacted, with carbonate rhyzolithes and gradual transition downwards. The BCk horizon is light brown, compacted, with diffused coatings of clay on prismatic pedological structures. It comprises white spots of carbonate and rhyzolithes, and rarely krotovinas filled with loess. By its morphological features, the soil resembles a calcaric cambisol. OSL sample PRI-1.9 was collected from the upper part of Vytachiv unit (Figs. 2–3).

The *Uday (ud) loess unit* (or L1LL2) (2.0–2.5 m) is light pale-yellowish coarse silt, less compacted compared to the overlying paleosol, structureless, with few krotovinas and rich in carbonates, including soft carbonate nodules at 2.5–2.6 m depth. The lower limit is gradual. Sample PRI-1.10 was collected from the middle of Uday unit.

The *Pryluky (pl) paleosol unit* (or S1SS1) (2.50–2.90 m) is a truncated brownish paleosol (the intensity of coloration increases downwards), compacted, with weak crumbly structure and gradual transition

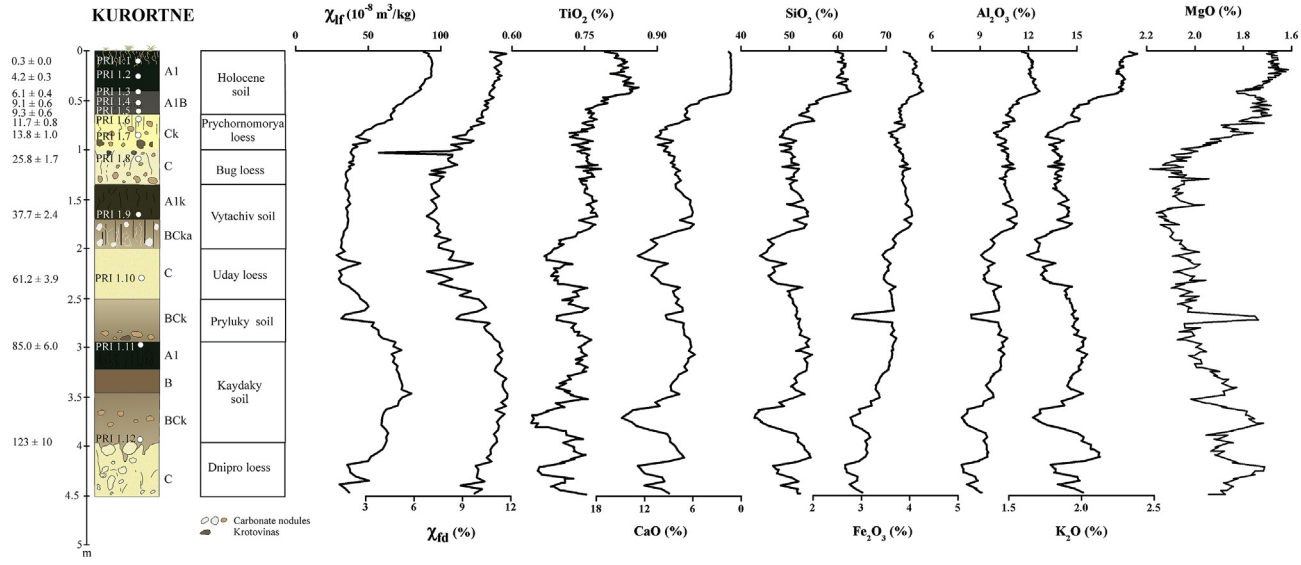

Fig. 2. The lithostratigraphy of the investigated uppermost 4.5 m at Kurortne loess-paleosol section, alongside the identified regional chronostratigraphic units of the Ukrainian Quaternary stratigraphic framework. The sedimentological data include the low-frequency magnetic susceptibility (χ_{lf}), frequency-dependent magnetic susceptibility (χ_{fd}) and the relative abundance (in %) of major oxides TiO_2, CaO, SiO_2, Fe_2O_3, Al_2O_3, K_2O, and MgO. Note the reversed horizontal axis for CaO and MgO. The location of OSL samples discussed in the main text and Table 1 is also indicated.

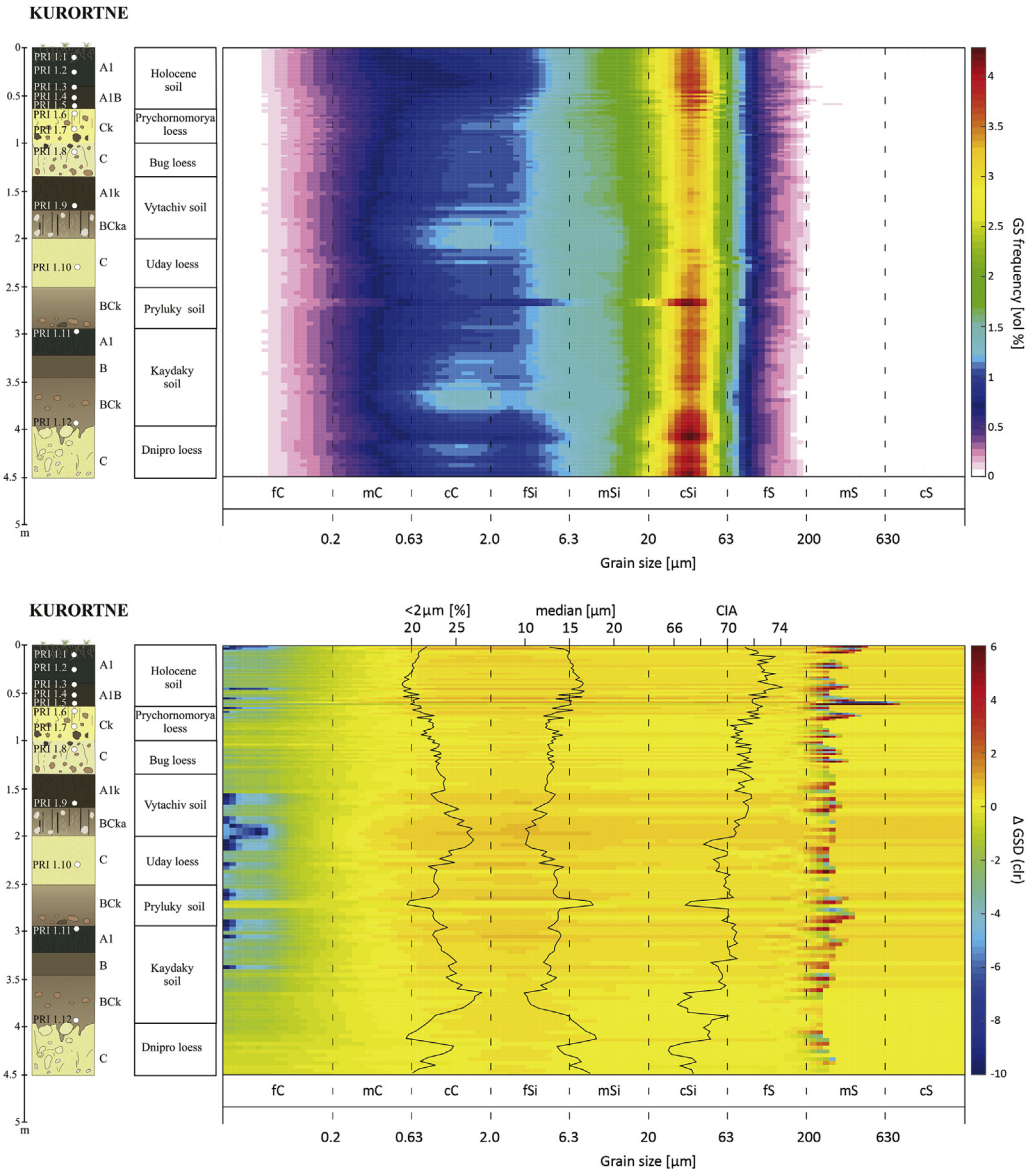

Fig. 3. Heatmap plot of grain-size variability for the 4.5 m investigated at Kurortne: a) Heatmap showing the classic grain size distribution of all samples; and b) Heatmap showing the ΔGSDclr (grain-size frequency calculated with the Fraunhofer approximation – GS frequency calculated with the Lorenz-Mie theory) of all samples plotted against depth; the ΔGSD is shown for each of the 116 grain-size classes resulting from the laser diffraction analysis. To deal with the compositional data effect, the distributions are analyzed as centered log ratio (clr)-transformed grain size differences (Schulte and Lehmkuhl, 2018). The vertical curves represent the clay fraction < 2 µm (%), the median GS (µm) and the CIA (CIA = [Al_2O_3/(Al_2O_3 + Na_2O + CaO* + K_2O)] * 100; CaO* is silicatic CaO, (Nesbitt and Young, 1982)).

downwards. It preserves smaller amounts of carbonates than the Uday loess in the BCk horizon that extends over the depth interval 2.70–2.85 m.

The *Kaydaky (kd) paleosol unit* (ie., S1SS2) (2.90–4.1 m) comprises three genetic horizons (Fig. 2). The A1 horizon is brownish-grey, significantly darker than the overlying Pryluky (pl) paleosol, composed of porous coarse silt, with weak structure, with rhyzolithes and desiccation cracks filled with the overlying material. The B-horizon is grayish-brown, porous, loose, with weak crumbly structure, dispersed secondary carbonates and a gradual lower boundary. The BCk horizon is brown, loose, with weak crumbly structure and "beloglazka" (soft carbonate nodules, up to 10 cm in diameter). The lower boundary is rather irregular, with soil aggregates penetrating down by patches (up to 30 cm in depth) and by cracks ("humus tongues", up to 50 cm in depth). Sample PRI-1.11 was collected from the transition between the Pryluky and Kaydaky units, whereas PRI-1.12 was sampled from the middle part of Kaydaky BCk horizon. The morphological and pedological characteristics (ie., the thickness of humified part of the profile, the position of carbonate horizon) of this chernozem allows attributing it to the subtype 'chernozem common' of the Ukrainian pedological framework (Poznyak, 2010).

The *Dnipro (dn) loess unit* (or L2LL1) was sampled only in the depth interval 3.90–4.5 m, but it extends up to 6 m depth comprising a light-yellowish silt, porous, loose, with no clear texture and tiny punctuations of manganese hydroxides.

3. Methods and instrumentation

3.1. Sedimentological analyses

As described above, contiguous sampling of the uppermost 4.5 m at Kurortne yielded 145 samples for sedimentological and geochemical analyses (Figs. 2–3). The rock magnetic measurement protocol follows Zeeden et al. (2018b) with the dried material filled into 6.4 cm^3 plastic boxes, compressed, and fixed with cotton wool to prevent movement of particles during analytical measurements at Bayreuth University, Germany. A susceptibility bridge (VFSM; Magnon, Germany) operating at AC-fields of 300 Am^{-1} at 0.31 kHz (ie., χlf) and 3 kHz (ie., χhf) was used for determining the magnetic susceptibility, reported here as mass specific susceptibility χ following density normalization. Maher (2011) suggested that χlf reflects variability in the concentration and magnetic grain size of loess ferrimagnetic minerals. When pedogenetic processes impact on the primary character of loess, the concentration of pedogenetically formed ultra-fine magnetic particles can be determined by

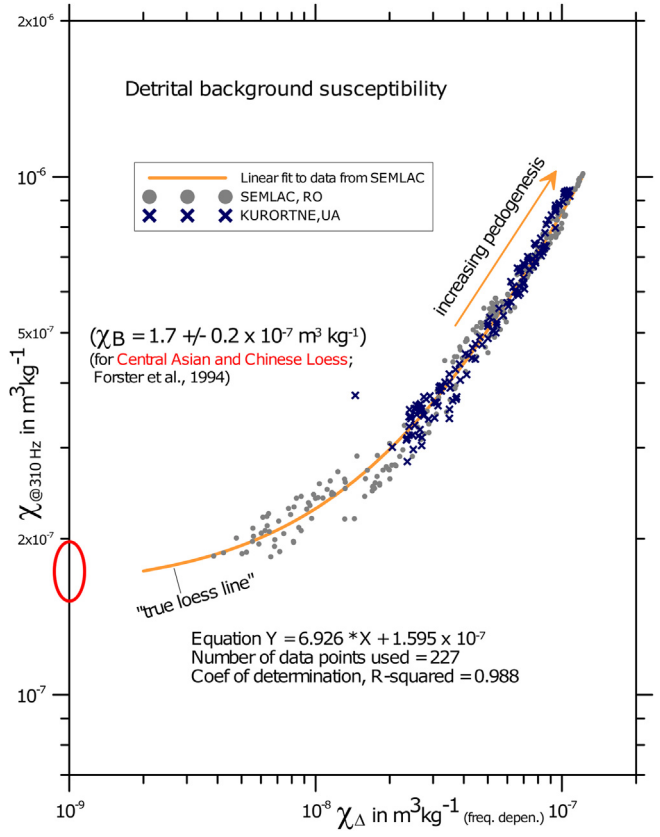

Fig. 4. Plot of the χ_{lf} (ordinate) versus χ_{Δ} (abscissa) for Kurortne, Ukraine (this study; crosses) and similar data from Semlac loess-paleosol sequence, southwestern Romania, as discussed in Zeeden et al. (2016). For location of sites see Fig. 1.

the frequency dependent magnetic susceptibility calculated as $\chi fd = (\chi lf - \chi hf)/\chi lf * 100$ [%] (Fig. 2) and $\chi\Delta = (\chi lf - \chi hf)$ [$kg^3\ m^{-1}$], respectively (see Zeeden et al., 2018b). The $\chi\Delta$ as function of χlf (Fig. 4) provides a measure of magnetic enhancement in the course of pedogenesis and has often also been employed in determining the detrital background susceptibility of unweathered parent loess; it is thus a proxy for inferring the impact of long-term hydroclimate variability on loess-paleosol records (see Forster et al., 1994; Buggle et al., 2014; Schaetzl et al., 2018).

The particle size distribution was measured with a Laser Diffraction Particle Size Analyzer (Beckman Coulter LS 13 320), by calculating the percentage size frequency of 116 classes within a size range of 0.04–2000 μm with an error of 2% (expressed by the coefficient of variation (CV); i.e., the standard deviation divided by the mean, reported as a percentage). Organic matter was removed by treating the samples with 0.70 ml 30% H_2O_2 at 70 °C for several hours. To keep particles dispersed, the samples were treated with 1.25 ml $Na_4P_2O_7$ (0.1 mol*l-1) for 12 h on an overhead shaker (ISO 11277, 2002; Schulte et al., 2016). Each sample was measured four times in two different concentrations to increase precision. The classic grain size distribution was determined by applying the Mie theory (Fluid RI: 1.33; Sample RI: 1.55; Imaginary RI: 0.1; Özer et al., 2010; ISO 13320, 2009cf. Schulte et al., 2016). In order to better visualize variability in grain size distribution, we present the grain size data as a heatmap (Fig. 3a).

There are two different recently common optical models to calculate the GSD from the light scattering pattern, the Fraunhofer approximation, and the Mie Theory. According to the Fraunhofer approximation, some of the light hitting a particle is diffracted in a grain size dependent angle. The angle of diffraction increases with decreasing grain size (Blott and Pye, 2006). Contrary to the Fraunhofer approximation, which takes only the diffraction at the particle surface into account, the Mie Theory also considers the complex refractive indices of the particles and the suspension fluid (ISO 13320, 2009). For the application of the Mie Theory, the refractive index of the fluid (here 1.33 for water) and the complex refraction index of the sample (m = n - ki, composed of the real component (n) reflecting the refraction within the particle and the imaginary component (ki) which considers the light absorption) have to be defined (Buurman et al., 1997; Schulte and Lehmkuhl, 2018). As the complex refraction index varies for different minerals (Haynes, 2015) and natural samples represent a polydisperse mineral mixture, a suitable medium value has to be implemented. In this study, the complex refraction index is fixed to m = 1.55 – i0.1 (Mishchenko, 1993; Özer et al., 2010). Nevertheless, because of the polymineral composition of loess samples, in particular, in the case of post-depositional altered minerals, the optical properties may differ considerably and the occurrence of artifacts in the fine range is unavoidable.

Since the scattering at particles larger than ten times the wavelength of the light source (in the case of the Beckman Coulter LS 13320: 10*780 nm = 7.8 μm), the grain size distribution in the coarser range is rather independent of the complex refractive index (McCave and Syvitski, 1991; Lagasse and Richards, 2003). In contrast, in the submicron range, where pedogenically formed minerals are enriched, substantial differences occur between the calculated GSDs of both models. In fact, neither of the common optical models provides the true size of the submicron particles. However, with increasing chemical weathering, the proportion of podogenically formed minerals (which are poorly represented by the complex refractive index) increases in the submicron range at the expense of a decrease in primary minerals (which are well represented by the complex refractive index).

During accumulation, loess consists mainly of coarse silt, whereas particles < 1 μm are extremely underrepresented (Qiang et al., 2010; Újvári et al., 2016; Schulte and Lehmkuhl, 2018). The variability of the difference of both optical models (ΔGSD) is a strong estimator for the degree of post-depositional GS fractionation due to chemical weathering processes. To deal with the compositional data effect (Aitchison, 1986), the distributions are analyzed as centered log ratio (clr)-transformed grain size differences (ΔGSDclr; Fig. 3b). The transformed dataset is more robust against other grain size influencing processes especially during sediment accumulation (sheet wash, saltation or enhanced background sedimentation). For detailed information, see Schulte and Lehmkuhl (2018).

In order to assess the long-term geochemical variability at Kurortne, the concentration of selected elements was measured on the fine-grained fractions extracted by sieving out material < 63 μm and drying it at 105 °C for 12 h. Eight grams of the sieved material was mixed with 2 g Fluxana Cereox, homogenized, and pressed to a pellet with a pressure of 20 tons for 120 s. All samples were measured twice with a SpectroXepos X-ray fluorescence (XRF) device. Subsequently, mean values were calculated from the two measurements following the instructions of Spectro (2007), and variability in selected major oxide data is discussed in Fig. 2. To estimate the degree of weathering, the chemical index of alteration (CIA) was calculated according to Nesbitt and Young (1982): $CIA = [Al_2O_3/(Al_2O_3 + Na_2O + CaO^* + K_2O)] * 100$ (in molar proportions; CaO* refers to silicatic Ca).

3.2. Optically stimulated luminescence (OSL) dating

3.2.1. Preparation of luminescence samples

The luminescence samples were prepared in the laboratory under low intensity red light conditions at Babeș-Bolyai University luminescence dating laboratory, Cluj-Napoca, Romania. Sampling was performed by hammering stainless steel cylinders perpendicularly onto two freshly cleaned vertical exposures. The material at each end of the cylinders was extracted for high-resolution gamma spectrometry measurements and water content estimations. Relative moisture was estimated for each sample. Hydrochloric acid (35% concentration) was

Table 1
Summary of the luminescence and dosimetry data. Weighted OSL ages are calculated according to Aitken (1985). The uncertainties associated with the luminescence and dosimetry data are random; the uncertainties mentioned with the optical ages are the overall uncertainties. All uncertainties represent 1σ. The ages were determined considering the "as found" water content, with a relative error of 25%; n denotes the number of accepted aliquots; beta attenuation and etching factor used for 63–90 μm and 90–125 μm fractions are 0.94 ± 0.050 and 0.92 ± 0.050, respectively; adopted alpha efficiency factor was 0.04 ± 0.02. The total dose rate consists of the contribution from the alpha, beta and gamma radiations as well as the contribution from the cosmic radiation.

Sample code	Depth (cm)	Grain size (μm)	Water content (%)	ED (Gy)	U–Ra (Bq/kg)	Th (Bq/kg)	K (Bq/kg)	Total random error (%)	Total Systematic error (%)	Total dose rate (Gy/ka)	Age (ka)	Weighted ages (ka)
PRI 1.1	15	4–11	4.4	3.5 ± 0.1 (n = 11)	42.8 ± 1.3	40.6 ± 1.2	508 ± 15	3.2	7.9	4.00 ± 0.06	0.9 ± 0.1	0.3 ± 0.0
		63–90		1.1 ± 0.1 (n = 10)				9.2	5.5	3.36 ± 0.05	0.3 ± 0.0	
		90–125		0.8 ± 0.1 (n = 10)				12.6	5.4	3.32 ± 0.05	0.2 ± 0.0	
PRI 1.2	30	4–11	6.2	15.4 ± 0.1 (n = 11)	41.3 ± 1.5	39.4 ± 1.5	507 ± 14	1.8	7.9	3.83 ± 0.06	4.0 ± 0.3	4.2 ± 0.3
		63–90		14.7 ± 1.4 (n = 10)				9.7	5.6	3.22 ± 0.05	4.6 ± 0.5	
		90–125		13.8 ± 1.1 (n = 12)				8.1	5.6	3.18 ± 0.05	4.3 ± 0.4	
PRI 1.3	43	4–11	2.8	24.0 ± 0.7 (n = 11)	38.6 ± 0.1	41.6 ± 1.1	485 ± 16	3.3	7.9	3.87 ± 0.06	6.2 ± 0.5	6.1 ± 0.4
		63–90		24.1 ± 2.3 (n = 10)				9.7	5.4	3.24 ± 0.05	7.4 ± 0.8	
		90–125		17.2 ± 1.4 (n = 12)				8.3	5.4	3.20 ± 0.05	5.4 ± 0.5	
PRI 1.4	53	4–11	2.2	30.4 ± 0.4 (n = 10)	37.0 ± 0.9	33.4 ± 0.8	447 ± 13	2.0	7.8	3.52 ± 0.05	8.6 ± 0.7	9.1 ± 0.6
		63–90		28.7 ± 2.0 (n = 10)				7.1	5.4	2.96 ± 0.05	9.7 ± 0.9	
		90–125		26.7 ± 1.4 (n = 12)				5.5	5.4	2.92 ± 0.05	9.1 ± 0.7	
PRI 1.5	58	4–11	6.7	32.6 ± 0.7 (n = 11)	37.3 ± 0.3	35.2 ± 0.3	453 ± 13	2.5	8.0	3.41 ± 0.04	9.6 ± 0.8	9.3 ± 0.6
		63–90		26.6 ± 1.5 (n = 11)				5.8	5.6	2.87 ± 0.04	9.3 ± 0.8	
		90–125		26.2 ± 1.0 (n = 12)				4.1	5.6	2.83 ± 0.04	9.2 ± 0.6	
PRI 1.6	68	4–11	6.5	39.5 ± 0.4 (n = 12)	38.2 ± 1.4	35.5 ± 1.3	496 ± 16	2.1	7.8	3.58 ± 0.07	11.0 ± 0.9	11.7 ± 0.8
		63–90		37.9 ± 1.6 (n = 10)				4.6	5.7	3.02 ± 0.06	12.5 ± 0.9	
		90–125		34.8 ± 2.6 (n = 12)				7.7	5.6	2.99 ± 0.06	11.7 ± 1.1	
PRI 1.7	85	4–11	8.5	42.9 ± 0.5 (n = 10)	36.1 ± 1.0	33.4 ± 1.3	448 ± 12	2.0	8.1	3.25 ± 0.05	13.2 ± 1.1	13.8 ± 1.0
		63–90		41.8 ± 2.6 (n = 11)				6.4	5.8	2.74 ± 0.04	15.3 ± 1.3	
		90–125		36.1 ± 2.5 (n = 10)				7.1	5.8	2.70 ± 0.04	13.4 ± 1.2	
PRI 1.8	115	4–11	7.7	89.4 ± 1.1 (n = 10)	38.0 ± 1.1	39.4 ± 0.5	447 ± 13	1.8	8.3	3.45 ± 0.05	25.9 ± 2.2	25.8 ± 1.7
		63–90		88.7 ± 4.0 (n = 10)				4.7	5.7	2.88 ± 0.04	30.8 ± 2.3	
		90–125		62.8 ± 4.1 (n = 12)				6.7	5.7	2.85 ± 0.04	22.0 ± 1.9	
PRI 1.9	150	4–11	4.2	123 ± 1 (n = 10)	33.1 ± 1.5	36.5 ± 1.0	458 ± 13	1.9	7.8	3.41 ± 0.06	36.2 ± 2.9	37.7 ± 2.4
		63–90		111 ± 5 (n = 10)				4.9	5.5	2.87 ± 0.05	38.7 ± 2.8	
		90–125		108 ± 4 (n = 12)				3.8	5.5	2.84 ± 0.05	38.0 ± 2.5	

(*continued on next page*)

Table 1 (*continued*)

Sample code	Depth (cm)	Grain size (μm)	Water content (%)	ED (Gy)	U–Ra (Bq/kg)	Th (Bq/kg)	K (Bq/kg)	Total random error (%)	Total Systematic error (%)	Total dose rate (Gy/ka)	Age (ka)	Weighted ages (ka)
PRI 1.10	227	4–11	1.5	218 ± 1 (n = 11)	36.5 ± 0.4	40.0 ± 0.7	458 ± 14	1.5	8.0	3.68 ± 0.05	59.3 ± 4.8	61.2 ± 3.9
		63–90		210 ± 10 (n = 14)				5.2	5.4	3.07 ± 0.05	68.5 ± 5.1	
		90–125		177 ± 6 (n = 22)				3.8	5.4	3.03 ± 0.05	58.3 ± 3.8	
PRI 1.11	295	4–11	6.7	248 ± 1 (n = 11)	32.8 ± 1.3	39.9 ± 1.0	472 ± 15	1.8	8.0	3.41 ± 0.06	72.8 ± 6.0	–
		63–90		243 ± 9 (n = 10)				4.2	5.7	2.86 ± 0.05	85.0 ± 6.0	
		90–125		235 ± 13 (n = 12)				5.8	5.7	2.83 ± 0.05	83.0 ± 6.7	
PRI 1.12	375	4–11	9.7	283 ± 3 (n = 10)	28.7 ± 0.2	33.4 ± 1.5	461 ± 15	2.1	7.9	3.01 ± 0.06	94.2 ± 7.7	–
		63–90		313 ± 15 (n = 10)				5.2	6.0	2.55 ± 0.05	123 ± 10	
		90–125		280 ± 11 (n = 10)				4.5	6.0	2.52 ± 0.05	111 ± 8	

applied in order to remove carbonates, followed by a hydrogen peroxide (H_2O_2, concentration of 30%) treatment for organic matter removal. The coarse grain fractions (63–90 μm and 90–125 μm) were separated through dry sieving. The material was treated with 40% HF for 40 min, followed by a 60 min bath in 10% HCl and a final dry sieving. For measurement, the coarse quartz grains 63–90 μm and 90–125 μm separates were mounted on stainless steel disks and silicon oil was used as adhesive. The fine fraction (4–11 μm) was separated by settling in Attenberg cylinders followed by applying an etching treatment with 35% H_2SiF_6 for 10 days. The 4–11 μm quartz fraction was mounted on aluminium disks from a suspension in acetone (2 mg/ml).

3.2.2. Equivalent dose determination

Investigations were carried out on three quartz grain size separates (4–11 μm, 63–90 μm and 90–125 μm) per sample, in order to verify the overall dating accuracy and for obtaining weighted average ages that better reflect the time of sediment deposition. Luminescence measurements were carried out using two Risø TL/OSL-DA-20 readers equipped with classic or automated detection and stimulation heads (DASH) (Lapp et al., 2015), whereas luminescence signals were detected by EMI 9235QA and PDM 9107Q-AP-TTL-03 photomultiplier tubes (Thomsen et al., 2006). Laboratory irradiations were carried out using the incorporated ^{90}Sr-^{90}Y radioactive sources, calibrated against gamma irradiated calibration quartz supplied by Risø National Laboratory, Denmark (Hansen et al., 2015). The dose rates used for the coarse (63–90 μm and 90–125 μm) quartz grains deposited on stainless steel disks were 0.130 Gy/s and 0.088 Gy/s, respectively. The dose rate for the fine grains mounted on aluminium disks was 0.078 Gy/s at the time of measurement.

Luminescence characteristics of fine (4–11 μm) and coarse (63–90 μm and 90–125 μm) quartz grains were analyzed using the single-aliquot regenerative dose (SAR) protocol (Murray and Wintle, 2000, 2003). Optical stimulation was carried out with blue light emitting diodes for 40 s at 125 °C, while the signals were recorded through a 7.5 mm thick Hoya U-340 UV filter. The net CW-OSL signal was evaluated from the first 0.308 s of the decay curve with an early background subtraction assessed from the 1.69–2.30 s interval (Cunningham and Wallinga, 2010). Sensitivity changes were corrected using the OSL response to a test dose of 17 Gy throughout the whole set of measurements. A preheat temperature of 220 °C for 10 s and a cutheat of 180 °C were employed. A high-temperature bleach was performed by stimulation with blue LEDs for 40 s at 280 °C at the end of each test dose signal measurement (Murray and Wintle, 2003).

The robustness of the SAR protocol was checked by the intrinsic performance tests (recycling and recuperation) (Murray and Wintle, 2003). The purity of the quartz grains extracted was evaluated on all aliquots measured using OSL IR depletion tests (Duller, 2003). Recycling and OSL IR depletion ratios within a maximum deviation of 10% from unity constituted the acceptance criteria along a recuperation signal amounting to less than 2% of the natural signal. In this study none of the investigated aliquots were rejected due to poor recycling, recuperation or IR depletion values.

3.2.3. Dosimetry

High-resolution gamma spectrometry was applied for determining the radionuclide activity concentrations. A hyperpure germanium well detector was used for measurements, having a volume of 120 cm^3, full width at half maximum (FWHM) at 122 keV of 1.40 KeV and a full width at half maximum (FWHM) at 1332 KeV of 2.30 KeV. The dose rates were derived based on the conversion factors reported by Adamiec and Aitken (1998). An alpha efficiency factor of 0.04 ± 0.02 was assumed for the 4–11 μm quartz fraction, to account for the lower efficiency of alpha radiation in inducing luminescence (Rees-Jones, 1995). For 63–90 μm and 90–125 μm quartz fractions, the beta attenuation and etching factors were assumed to be 0.94 ± 0.05 and 0.92 ± 0.05, respectively (Mejdahl, 1979). The cosmic ray component of the dose

rate was determined according to equations published by Prescott and Hutton (1994). Water content estimation was obtained based on the difference between the raw and the oven-dried weight of material with a relative error of 25%. An internal dose rate of 0.01 ± 0.002 Gy/ka was considered (Vandenberghe et al., 2008). The values for the total dose rates as well as the radionuclide concentrations for these samples are given in Table 1.

4. Results and discussion

4.1. Sedimentological and geochemical data

The magnetic susceptibility (χ) and its field-depended component (χ_{fd}) are reliable indicators for the intensity of pedogenesis and chemical weathering of primary loess (Forster et al., 1994; Buggle et al., 2014). The χ record of Kurortne LPS shows high values for paleosols and lower values in loess, varying between 28 10^{-8} m^3/kg (the Uday loess) to 94 10^{-8} m^3/kg (the Holocene soil) (Fig. 2). The lowermost Dnipro loess unit shows low χ_{lf} values, which strongly increase in the Kaydaky paleosol, especially in the upper part of BCk horizon and throughout the B-horizon (Fig. 2). The Pryluky paleosol shows lower values than the Kaydaky unit with a sharp dip at 2.70–2.75 m depth that is also recorded in other proxies (Figs. 2–3). The χ_{lf} for Uday loess is low, except a distinctive peak around 210–220 cm depth reflected also in other data (Fig. 3). The Vytachiv paleosol shows lower values than the two older paleosol units. The χ_{lf} values are low in the Bug loess; they start to increase significantly at the depth of 1 m. The χ_{fd} parallels the trend in χ_{lf} (Fig. 2), the two proxies being well correlated (R^2 = 0.648), but showing more variability in the Pryluky, Uday and Vytachiv units. χ_{fd} generally oscillates around 11% in the Kaydaky unit and the Holocene soil, reaching lower minima of 6–7% in the Vytachiv and Bug units (Fig. 2).

In general, X_{lf} is on the one hand controlled by the original background susceptibility probably acquired in the source area of the dust and by pedogenic magnetic enhancement due to the in-situ neo-formation of ultra-fine super-paramagnetic particles in the course of pedogenesis. High-frequency variations in dust input and/or in pedogenic overprint are unlikely to be recorded in low deposition rates settings due to low pass filter effects of both processes mentioned above (Anderson and Hallet, 1996), but control nevertheless the general level and trend of X_{lf}."

The similar low or even slightly higher values of X_{lf} in intervals of the Bug loess compared to parts of the Vychativ paleosol can be explained by such smeared out high-frequency climatic variations including short warm and moist intervals, which are typical for the late MIS3 to MIS 2 climatic trend (Fig. 2). Anderson and Hallet (1996) and more recently Zeeden et al. (2020) proposed and tested models which demonstrate that high-frequency variations in dust input and/or in pedogenic overprint are unlikely to be recorded in low deposition rates settings due to low pass filter effects of both processes mentioned above. Furthermore, a magnetic susceptibility threshold at Kurortne can be discerned at the end of the proper loess formation of the Bug unit. Thus, it is possible to place around 1 m depth the end of the pleniglacial loess formation and the onset of pedogenic processes that lead to the formation of the incipient soils of the Middle Prychornomorya subunit, and subsequently to the formation of the Holocene S0 soil. Fig. 4 displays $\chi\Delta$ as function of χlf from Kurortne compared to data of the Semlac LPS (Romanian Banat), which covers the last 400 kyr and hence almost 4 complete glacial-interglacial cycles. All but one data points from Kurortne mark the same magnetic enhancement path and show an identical detrital background susceptibility as already derived for Semlac (Fig. 4). This points not only to a magnetically homogeneous source area of the dust but also to an astonishingly homogeneous magnetic granulometry as indicated by the constant slope of the “true loess line” (Zeeden et al., 2016, 2018b). The homogeneity of magnetic granulometry is in turn caused by similar temporal patterns of long-term hydroclimate variability on LPSs during the Pleistocene and is almost identical across the entire mid-latitude Eurasian loess belt ranging from China in the east to the Danube Basin in the west (Forster et al., 1994; Buggle et al., 2014; Schaetzl et al., 2018).

The heatmap discussed in Fig. 3a and b demonstrates all measured grain size frequencies of 116 classes. It is interesting to note that for the whole data set, the main component of the grain size distribution is in the cSi (ie., 20–63 μm) fraction. Except for thin intervals in the Holocene soil, there are no particles in the mS (200–630 μm), or cS (630–2000 μm) fractions (Fig. 3a). The fC (< 2 μm) fraction shows high values in the Kaydaky soil and at the transition from the Vytachiv soil to the Uday loess. The high proportion of the fraction < 2 μm may indicate clay production due to increased chemical weathering following pedogenetic overprinting, as would also be indicated by the χ vs. χ_{fd} plot (Fig. 6). The continuous increase in 2–20 μm fraction may reflect a long-term decrease in wind intensity. The > 63 μm fraction has the smallest proportion in the Kaydaky soil, and the 20–63 μm fraction shows low values both in the Kaydaky and Vytachiv paleosols.

The ΔGSD(clr) is used as a reliable indicator of post-depositional chemical weathering in LPS. In Fig. 3b the ΔGSD(clr) values are shown as a heatmap signature. The values of the ΔGSD(clr) signal for the submicron grain size range are low in the Prychornomorya loess, the Bug loess, the lower part of the Kaydaky paleosol and the Dnipro loess (Fig. 3b). In the humus and humus-transitional horizons of the Holocene soil and in the depth interval between 1.5 m and 3.5 m, the ΔGSD (clr) signals for the submicron range increase. The variability in these values partly follows the stratigraphy, increasing mainly in the Holocene soil genetic horizons (A1B) denoting intense chemical weathering. It is noticeable that the high values of < 2 μm fraction (3.60–3.80 m depth) within the Kaydaky paleosol are not followed by the ΔGSD(clr) signature, but by a significant increase in CaO and a prominent minina in CIA fact that might indicate less weathered material (Figs. 2 and 3a,b).

Fig. 2 shows the geochemical data denoting concurrent variability in all major oxides between paleosols and the loess units that is well reflected in the lithostratigraphy. The SiO_2 values ranges from 42.7% to 62.7% (average 52.3%), whereas Al_2O_3 varies between 7.8% and 12.7%, with an average of 10.4%. Other major oxides are present in smaller concentrations. The Fe_2O_3 content varies from 2.7% to 4.3% (average 3.7%). The K_2O and MgO contributions vary from 1.6% to 2.4% and 1.6%–2.4%, respectively, both elements have an average of 1.9%. TiO_2 contributes with 0.64–0.86% (average 0.75%), P_2O_5 with 0.13–0.21% (average 0.16%) and MnO is in the range of 0.05–0.11% (average 0.08%). CaO reaches values between 1.2% and 14.9% (average 7.5%) and it reflects well the lithostratigraphic changes, attaining highest values in both the Dnipro, Uday, and Bug loess units and the lower parts of Kaydaky and Vytachyv soils, and lowest values in the Holocene soil. As the trend in other major oxides is inversely correlated with CaO, it indicates that it renders a dilution effect, which can also be discerned when compared with χ (Fig. 2). An exception is the sharp variability at 2.70–2.75 m depth which is reflected as a drop/increase in most major oxides (and concordant variability in χ and grain-size; Figs. 2–3) except for SiO_2 and K_2O – this would indicate a potential presence of volcanic particles, as tephra layers have often been reported within southeastern European loess records (Constantin et al., 2012; Veres et al., 2013; Anechitei-Deacu et al., 2014; Marković et al., 2015, 2018). However, an alternative interpretation is presented in section 5.2.

4.2. Luminescence properties and equivalent doses

The equivalent doses (D_e) were obtained by projecting the sensitivity corrected natural OSL signal onto the dose response curve constructed for each luminescence sample (see Fig. 2 for downwall location of samples). Fig. 5 presents the representative SAR growth curves for a single aliquot of fine (4–11 μm) and coarse (63–90 μm and 90–125 μm)

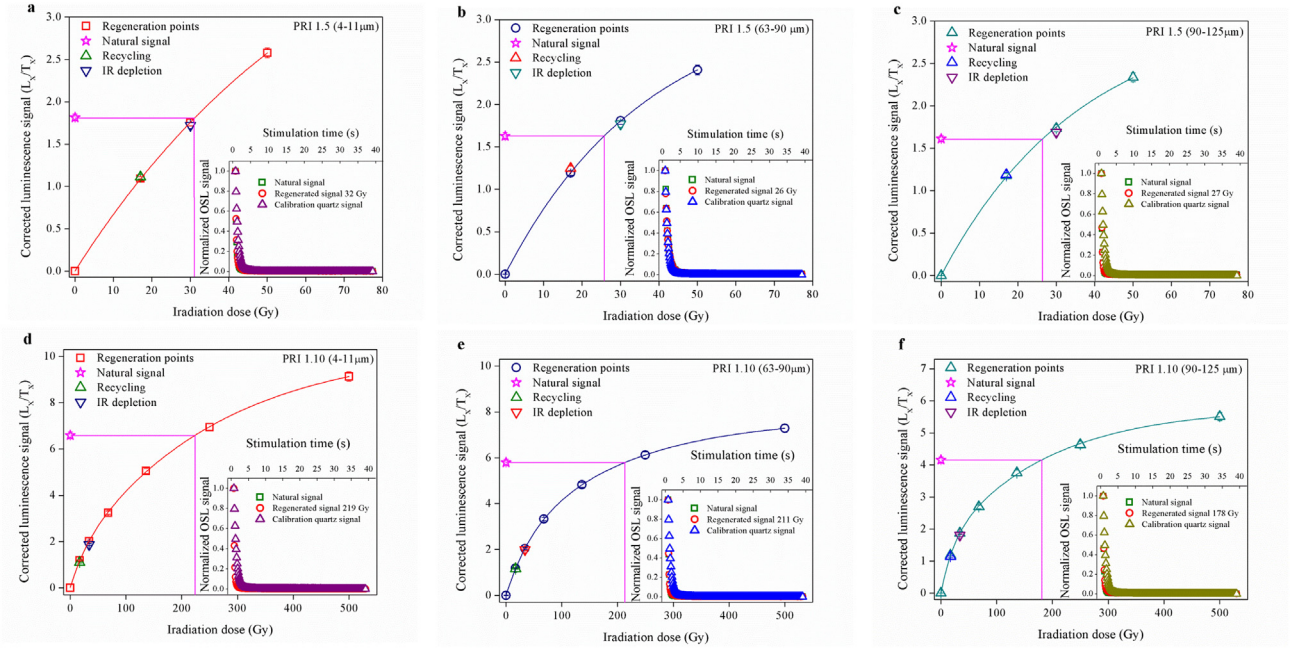

Fig. 5. Representative sensitivity-corrected growth curve constructed for (a), (d) 4–11 μm, (b), (e) 63–90 μm, and (c), (f) 90–125 μm quartz fractions from samples PRI-1.5 and PRI-1.10, respectively (See Figs. 2–3 for location of samples). The responses to regenerated doses are shown as open squares. The sensitivity corrected natural signal is depicted as a star, whereas the arrow indicates the equivalent dose. Recycling and IR depletion points are represented as an open triangle and an open down triangle, respectively. The inset shows a typical decay curve of natural CW-OSL signal (open squares) in comparison to a regenerated signal (open circles) and a calibration quartz signal (open triangles).

grained quartz from samples PRI-1.5 and PRI-1.10. The OSL signals displayed a rapid decay in the case of both fine and coarse quartz aliquots during optical stimulation, the shapes of the OSL decay curves being almost identical to those obtained for the calibration quartz supplied by the Risø National Laboratory (see inset to Fig. 5).

Furthermore, the dependency of the equivalent doses on the preheat temperature was investigated for sample PRI-1.7. Aliquots of fine (4–11 μm) and coarse (63–90 μm) quartz were separated into groups of five, each corresponding to a temperature point (ie., 180 °C, 200 °C, 220 °C, 240 °C, 260 °C, 280 °C). A 180 °C cutheat (test dose preheat) was employed. As shown in Supplementary File Fig. S2, the preheat plateau indicates the thermal stability of the OSL signal and ensures that any thermal transfer is irrelevant. The recycling ratio and recuperation were satisfactory for all measured aliquots.

Further on, dose recovery tests (Murray and Wintle, 2003) were conducted to investigate the reliability of the equivalent doses obtained by applying the SAR protocol on fine (4–11 μm) and coarse (63–90 μm) quartz grains from samples PRI-1.2, 1.4, 1.6, 1.8 and PRI-1.10. The test consisted in double bleach for 250 s at room temperature using the blue LEDs with a 10 ka pause inserted between the stimulation. The aliquots were then irradiated with known beta doses chosen to be equal to the estimated equivalent doses, and measured using the SAR protocol. As seen in Supplementary File Fig. S3, very good recovery to given dose ratios were obtained, except for PRI-1.2 (4–11 μm quartz fraction) showing 14% underestimation.

Dose response for very high doses was investigated using three aliquots from PRI-1.12 (Dnipro loess), and sensitivity corrected growth curves extending up to 5000 Gy were constructed on fine (4–11 μm) and coarse (63–90 and 90–125 μm) quartz grains (Supplementary File Fig. S1). The growth curve was best fitted by a sum of two saturating exponential function such as in the following equation:

$$I(D) = I_0 + A(1 - \exp(-D/D_{01})) + B(1 - \exp(-D/D_{02}))$$

where, I is the intensity of the signal for a given dose D, I_0 is the intercept, A and B are the saturation intensities of the two exponential components and D_{01}, D_{02} are the dose levels characteristic of the dose–response curve of each exponential function (Wintle and Murray, 2006), parameters which we will refer to as saturation characteristics.

From data in Supplementary File Fig. S1 it can be observed that the fine quartz fraction (4–11 μm) saturates at significantly higher doses than coarse (63–90 μm and 90–125 μm) fractions. From doses higher than about 100 Gy a significant difference in the response between fine and coarse-grained quartz was observed. Different saturation characteristics of fine and coarse quartz grains have been reported previously in loess samples from southeastern Europe and the Chinese Loess Plateau (CPL) (Timar-Gabor et al., 2012, 2015; 2017). For the 4–11 μm quartz fraction of sample PRI-1.12 we are reporting average values for the saturation characteristics of D_{01} = 170 Gy and D_{02} = 1355 Gy, for the 63–90 μm fraction the corresponding values are D_{01} = 41 Gy and D_{02} = 316 Gy, whereas in the case of 90–125 μm fraction, saturation characteristics of D_{01} = 44 Gy and D_{02} = 390 Gy were determined. Our results are similar with the saturation characteristic doses reported by Timar-Gabor et al. (2017) for worldwide loess and samples of various sedimentary origins (for 4–11 μm fine grains the values for D_{01} and D_{02} were 151 and 1411 Gy, respectively; for 63–90 and 90–125 μm coarse grains the values of D_{01} were 44 and 36 Gy, respectively, and for D_{02} 452 and 363 Gy, respectively).

Equivalent doses were determined on minimum ten aliquots of each grain size separate. Results of equivalent dose measurements and standard SAR performance tests (recycling, IR depletion and recuperation) are presented in Supplementary File Table S1. The equivalent doses obtained for the fine fraction (4–11 μm) are higher than the equivalent doses obtained on coarse quartz (except for the oldest sample PRI-1.12), as expected due the contribution of the alpha dose (Table 1, Supplementary File Table S1). We consider the equivalent doses obtained on fine quartz on the two oldest samples (PRI-1.11 and 1.12) as underestimates based on (i) comparison with coarse quartz data, and (ii) widely reported underestimation of equivalent dose beyond 100 Gy for loess samples from southeastern Europe and China (Timar-Gabor et al., 2017).

4.3. OSL ages and validity of regional correlations based on luminescence data

Table 1 presents a summary of the age results, with uncertainties on the individual ages obtained based on the error assessment system by Aitken and Alldred (1972) and Aitken (1976). The systematic errors account to maximum 6% for ages derived from coarse grains, and 8% for fine grains, respectively. The systematic error is particularly related to our estimates of the uncertainties associated with the time-averaged water content, beta attenuation, and alpha efficiency factors. The random error represents a measure of the internal consistency of the optical ages and extended to 13% for the coarse quartz grains (Table 1). For the fine grains the random error does not exceed 3%. The weighted average fine and coarse quartz ages were calculated (except for PRI-1.11 and 1.12) following Aitken's (1985) Appendix Band reported in Table 1.

For samples PRI-1.12 and 1.11 collected in the BCk horizon of the Kaydaky paleosol and at the Pryluky–Kaydaky soil boundary, coarse (63–90 μm) quartz ages 123 ± 10 ka and of 85 ± 6 ka, respectively, were obtained. These ages would confirm the correlation of Kaydaky and Pryluky paleosol units with MIS 5 (Rousseau et al., 2001; Gerasimenko, 2004, 2006; Buggle et al., 2009; Veres et al., 2018) (Fig. 6). The OSL ages obtained for the transition between the Pryluky and Kaydaky units broadly agree with the OSL ages of 70.1 ± 4.0 ka (D_e = 184 ± 9 Gy) and 93.6 ± 5.6 ka (D_e = 184 ± 9 Gy) obtained on 90–125 μm quartz grains, reported by Gozhik et al. (2014) for Pryluky unit in the Maxymivka section, situated in the Dnieper Plain. In the same profile, TL ages of 184 ± 27 ka (D_e = 475 ± 47 Gy) and 169 ± 25 ka (D_e = 339 ± 34 Gy) on 80–100 μm quartz grains were obtained for the Kaydaky unit (Gozhik et al., 2014), correlating this unit with MIS 7. Nevertheless, previous studies on the Ukrainian LPS deposits have reported that TL ages were overestimated (Kusiak, 2007; Łanczont et al., 2013). Moreover, similar studies conducted on Chinese loess have also reported age overestimation for loess samples dated through thermoluminescence methods (Buylaert et al., 2006; Lai et al., 2006).

The ages reported for the Pryluky-Kaydaky paleosols at Kurortne are in a very good agreement with results obtained on several LPS sequences at the Black Sea in Romania, where the paleosol (ie., S1) underlying the uppermost loess (L1) unit was correlated to MIS 5 (Timar et al., 2010; Timar-Gabor et al., 2011; Constantin et al., 2014). For instance, the coarse (63–90 μm) quartz OSL-ages at Kurortne are in agreement with OSL-ages of 94 ± 11 ka (D_e = 270 ± 27 Gy), 116 ± 11 ka (D_e = 334 ± 23 Gy) and 121 ± 10 ka (D_e = 342 ± 18 Gy), obtained on the same grain size from three samples collected from the S1 paleosol at Costinesti LPS (also at Black Sea, SE Romania) correlated with MIS 5 (Constantin et al., 2014) (Fig. 6). For samples collected immediately below and above the S1 paleosol at Mircea Vodă (Dobrogea, SE Romania), ages of 106 ± 16 ka (D_e = 310 ± 10 Gy) and 68 ± 10 ka (D_e = 221 ± 5Gy) were obtained for 4–11 μm quartz grains, whereas for 63–90 μm quartz grains, ages of 132 ± 18 ka (D_e = 319 ± 15 Gy) and 86 ± 11 ka (D_e = 237 ± 6 Gy) were obtained (Timar et al., 2010; Timar-Gabor et al., 2011). Furthermore, at Mostiştea (Lower Danube Plain, SE Romania), ages of 144 ± 21 ka (D_e = 391 ± 28 Gy) and 97 ± 14 ka (D_e = 227 ± 15 Gy) were obtained for 63–90 μm quartz grains on samples bracketing the S1 paleosol (Vasiliniuc et al., 2011).

The weighted average age of 61.2 ± 3.9 ka yielded for the Uday loess sample attributes this unit to the lower pleniglacial (MIS 4; Fig. 6) and agrees within errors with the TL-age of 65.9 ± 10 ka (D_e = 128.5 ± 13.2 Gy), obtained on 80–100 μm quartz grains reported by Gozhik et al. (2014). Thus it is very likely that the early pleniglacial at Kurortne corresponds to the Uday unit.

Sample PRI-1.9, collected from A1k horizon of Vytachiv unit at Kurortne, provided a weighted average age of 37.7 ± 2.4 ka. The available ^{14}C and luminescence data on the Vytachiv paleosol unit in the Middle Dnieper area (Gerasimenko, 2004; Bokhorst et al., 2011; Rousseau et al., 2011; Kadereit and Wagner, 2014) further enable the broad correlation of this unit with MIS 3. This is further supported by radiometric data discussed in Gozhik et al. (2014) that suggested the better-resolved Vytachiv unit at the Maxymivka sequence comprises most of MIS 3. The reported OSL ages of 53.8 ± 2.2 ka (D_e = 111.8 ± 3.1 Gy) and 24.9 ± 1.9 ka (D_e = 55.6 ± 2.7 Gy) were obtained on 90–125 μm quartz grains on samples closely

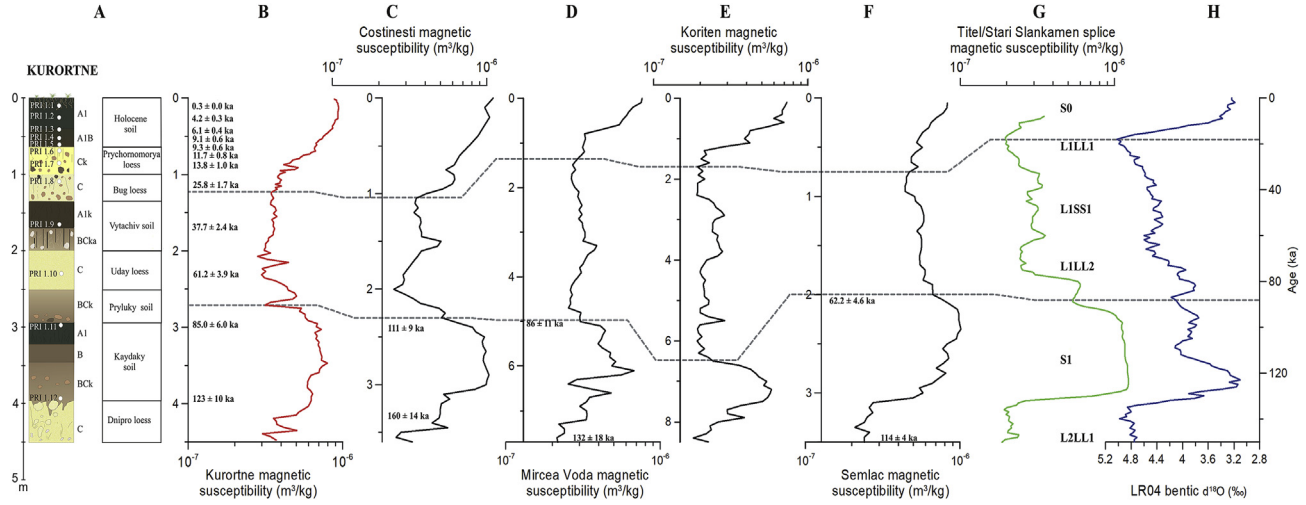

Fig. 6. Litho- and pedostratigraphical columns vs. magnetic susceptibility (χ_{lf}) record and OSL ages of the Kurortne loess-paleosol sequence (A, B), and its correlations to loess magnetic susceptibility (χ_{lf}) records of sites from the Middle and Lower Danube basins (C: Costinesti, Romania (Constantin et al., 2014; Necula et al., 2015); D: Mircea Vodă, Romania (Necula et al., 2013; Timar-Gabor et al., 2011); E: Koriten, Bulgaria (Jordanova and Petersen, 1999); F: Semlac, Romania (Zeeden et al., 2016) and to the astronomically tuned magnetic susceptibility record from the (G) Titel/Stari Slankamen (Serbia) composite record (Basarin et al., 2014) and the (H) benthic oxygen isotope stack (Lisiecki and Raymo, 2005). The Danube Basin loess stratigraphic nomenclature follows Marković et al. (2015). The dashed grey lines indicate stratigraphic correlation levels based on characteristic susceptibility patterns shared between the records. The OSL ages at Costinesti shown represent the weighted average ages of samples CST 11, CST 12, CST 13 (upper part of S1) and weighted average ages of CST 15, CST 16, CST 17 samples (upper part of L2 loess) obtained on 63–90 μm quartz extracts (Constantin et al., 2014). The OSL ages at Mircea Vodă were obtained on 63–90 μm quartz extracts (Timar-Gabor et al., 2011). The OSL ages at Semlac were obtained on 40–63 μm quartz extracts (upper part of S1) and 4–11 μm (lower part of S1), respectively (Zeeden et al., 2016). For location of sites please refer to Fig. 1.

bracketing the Vytachiv unit. At Stayky, also located in Middle Dnieper area, Veres et al. (2018) also attributed the truncated Vytachiv paleosol unit to within middle to late MIS 3. For the two samples roughly bracketing the Vytachiv paleosol OSL-ages of 34.6 ± 2.7 ka (D_e = 101 ± 5 Gy) and 26.0 ± 1.9 ka (D_e = 77.1 ± 2.3 Gy) were obtained for quartz grains of 63–90 μm. For 4–11 μm quartz grains, ages of 34.9 ± 3.3 ka (D_e = 121 ± 2 Gy) and 23.9 ± 2.0 ka (D_e = 81.7 ± 0.9 Gy) were reported (Veres et al., 2018).

It shall be noted however that in some sequences, the Vytachiv unit consists of three paleosols (Gerasimenko, 2006, 2011; Gozhik et al., 2014). The distinct peaks in the ΔGSD(clr) signal (Holocene soil, 1.5–2.0 m and 2.5–3.6 m) as well trends in several major oxides (e.g. CaO, SiO_2 or K_2O) and the CIA (Figs. 2–3) suggest that weak but distinct phases of pedogenesis could be distinguished at Kurortne. In other sections, the middle Vytachiv soils were IRSL-dated to 36.9 ± 3.4 ka (Bokhorst et al., 2011) and ESR-dated to 36 ± 3 ka and 38 ± 4 ka, respectively (Chabai and Monigal, 1999).

The weighted average age 25.8 ± 1.7 ka for the Bug loess unit allows its correlation with the upper pleniglacial (MIS 2) (Fig. 6). This age is in agreement with OSL ages of 25.8 ± 1.3 ka (D_e = 56.6 ± 2.3 Gy) and 21.1 ± 0.9 ka (D_e = 43.4 ± 1.4 Gy) obtained on 90–125 μm quartz grains from the two samples collected from the lower and upper part of the Bug unit elsewhere (Gozhik et al., 2014). The dates obtained on the Bug loess at Stayky in the Middle Dniper area (Rousseau et al., 2011; Veres et al., 2018) also are in agreement with a MIS 2 age.

For samples taken from the Holocene soil and over the transition to the Bug loess (Figs. 2–3), weighted average ages ranging from 0.3 ka to 13.8 ka have been obtained (Fig. 6). The A1 and A1B horizons of the Holocene soil yielded ages ranging from 0.3 ka to 9.3 ka, whereas the transitional horizon Ck has been dated between 11.7 ka and 13.8 ka (Fig. 6). The transition from the Pleistocene loess to the Holocene soil was identified on the basis of magnetic susceptibility threshold at around 1 m depth, thus prior to 13.8 ka (Fig. 6). Thus, the OSL ages show that the onset of magnetic susceptibility enhancement at Kurortne precedes the accepted stratigraphic Pleistocene-Holocene boundary dated at 11.7 ka in ice core records (Rasmussen et al., 2014). Similar results have been reported by Constantin et al. (2019) for Roxolany site in Ukraine, as well as in loess-paleosol sites across Romania and Serbia. The slight increase in values of the ΔGSD(clr) signal starting from the depth of 1 m in the section supports the assertion on the onset of significant soil formation prior to the Pleistocene-Holocene boundary at 11.7 ka, but likely concordant with the Late Glacial environmental changes (Rasmussen et al., 2014).

4.4. Regional correlations based on lithological, pedological and environmental magnetic data

The correlation of the Ukrainian stratigraphic units Uday loess, Vytachiv paleosol complex and Bug loess to MIS 4, MIS 3 and MIS 2, respectively, was reported in the previous investigations based on pedostratigraphical, palynological and magnetic susceptibility data (Gozhik et al., 2000, 2001, 2014; Rousseau et al., 2001, 2011; Gerasimenko, 2004, 2011; Buggle et al., 2008, 2009; Bokhorst et al., 2011; Veres et al., 2018). Two opposite views exist however on the correlation of Pryluky, Tyasmyn, Kaydaky and Dnipro units with MIS stages (see Introduction), as well as on the overall stratigraphy of loess plateau sections in the Black Sea region. According to some authors (Gozhik et al., 1995, 2000; Nawrocki et al., 1999), the uppermost chernozem-type paleosol (ie., equivalent to the paleosol described at 2.90–4.1 m in our record; Figs. 2–3, 6) is related to the Dofinivka unit radiocarbon dated at Kurortne (Prymorske) to 16.3 ± 0.3 ^{14}C ka BP, and underlain by a thick Bug loess unit dated to 21–26 ^{14}C ka BP. Thus, this loess unit (ie., below 4.1 m in our profile; Fig. 6) is correlated with the earlier part of MIS 2, and the Dofinivka chernozem is regarded as an interstadial paleosol formed after the Last Glacial Maximum. For the other view (Vozgrin, 2001, 2005; Veklitch, 2018), based on pedostratigraphical correlations with other LPS along a network of records throughout Ukraine, the uppermost fossil chernozem of the Pleistocene sequences is correlated instead with Kaydaky unit (thus MIS 5), and the loess below with the Dnipro unit (thus equivalent to L2LL1; Marković et al., 2015).

Both our field and analytical data would confirm this second opinion as in the investigated section at Kurortne, the chernozem identified between 2.90 and 4.1 m depth (Fig. 6) is a well developed paleosol, which, judging from its thickness and the depth position of the carbonate horizon, belongs to the same genetic type of chernozems as the modern S0 chernozem (Krypskyi and Polupan, 1979). According to previous paleopedological studies (Sirenko and Turlo, 1986), the Kaydaky paleosols in the studied area are represented by chernozems of the subtype 'common'. The soils of the optimal phase of Dofinivka soil formation are chernozems of subtype 'southern', with much stronger carbonatization of their profiles (including the formation of a Ck horizon which is completely saturated by farinaceous forms of carbonates). In other cases, these Dofinivka soils are represented by kastanozems (Sirenko and Turlo, 1986). Both genetic types of aforenamed soils were formed under much drier hydroclimate conditions than experienced during the formation of S0 soil. Paleopedological indices of clay weathering (Veklitch et al., 1967, 1982) are much lower in the Dofinivka soils than in the Kaydaky soils, denoting colder conditions during the formation of the former compared to environments during the formation of the later unit, or even the modern climate (Sirenko and Turlo, 1986). Thus, it is compelling to assert that the Dofinivka soils should correspond instead to interstadial(s) event(s), and the well developed chernozem paleosol at Kurortne is not related to the Dofinivka unit but to Kaydaky unit. According to the χ data (Figs. 2, 4 and 6), it is the only paleosol which can be compared to the Holocene S0 and thus, to an interglacial-type soil. The slightly lower χ values in the Kaydaky unit as compared with the Holocene can be explained by the higher content of young organic matter and likely bacterial induced neoformation of magnetic particles in the Holocene soil which can lead to enhanced susceptibilities (Maher et al., 2010). As demonstrated by Radaković et al. (2019) for recent topsoils from a loess plateau in the Carpathian basin, "active" living uppermost soil horizons show the highest magnetic enhancement compared to lower horizons of the Holocene soil and also compared to the Pleistocene paleosols.

Furthermore, it has been shown previously (Veklitch, 1982, 2018; Sirenko and Turlo, 1986; Vozgrin, 2005; Gerasimenko, 2006, 2011; Matviishina et al., 2010) that the Tyasmyn loess unit occurs rarely in the Ukrainian LPS (or it has a very small thickness), thus the Pryluky (ie., S1SS1) and Kaydaky (ie., S1SS2) paleosol units are frequently welded without the Tyasmyn loess bed in-between. At Kurortne, the Pryluky unit is partly truncated (only the BCk horizon identifiable; Figs. 2–3) but, in general, in this area it is represented by chernozems of subtype 'southern' or by kastanozems (Sirenko and Turlo, 1986). This fits well to the pedological characteristics of the BCk soil horizon, related to the Pryluky unit at Kurortne. The χ values are lower in the Pryluky unit than in the interglacial Kaydaky unit (Figs. 2 and 6). In other higher resolution sequences, the Pryluky unit consists of three subunits, the middle of which is a thin loess bed 'pl_2' (Rousseau et al., 2001; Gerasimenko, 2004, 2006; Gozhik et al., 2014; Haesaerts et al., 2016). At Kurortne, the sharp drop in both χ and clays within the Pryluky unit might indicate the presence of the 'pl_2' loess material which is indistinguishable visually due to overprinting by post-depositional pedogenic processes.

The Uday loess unit (ie., L1LL2) likely corresponds to the climate cooling of the early pleniglacial as reflected in the sharp decrease in χ (Fig. 2). The increase in clay fraction in the upper part of the Uday loess (Fig. 3) could be compared with the increase in the < 1 μm fraction in the upper part of corresponding loess unit in other Ukrainian LPS and interpreted as postdepositional reworking from the overlying Vytachiv soil (Veklitch et al., 1967; Sirenko and Turlo, 1986; Gerasimenko, 2006,

2011; Matviishina et al., 2010). On the other hand, an increase in both clays and some major oxides (e.g., Al_2O_3 and Fe_2O_3; Fig. 2) in the Uday loess unit is also described in many sections in Ukraine and Russia. The fact that the Uday loess unit is more clayey and less enriched in coarse silt than Bug or Dniper loesses led the aforenamed authors to suggest less energetic wind speed at the beginning of the early pleniglacial.

As discussed previously, the upper part of the Vytachiv unit (i.e., L1SS1) as preserved at Kurortne can be related to the middle Vytachiv paleosol (it shall be noted that in most complete sections of the Vytachiv unit (Bokhorst et al., 2011; Bolikhovskaya and Molodkov, 2006; Gerasimenko, 1999, 2010), the middle soil of MIS 3 (Vytachiv) pedocomplex is dated between 36 and 38 ka BP, whereas the upper Vytachiv paleosol to 28–30 ka BP). The different paleosol horizons forming the Vytachiv unit (likely emplaced during MIS 3 according to loess paleoecological data; Gerasimenko, 2006, 2011; Gozhik et al., 2014) most likely correspond to interstadial events, and in general, they are characterized by low χ values (Rousseau et al., 2001; Buggle et al., 2008, 2009). Nevertheless, χ values are somewhat higher in the lower Vytachiv paleosol than in the middle one (Buggle et al., 2008, 2009; Bokhorst et al., 2011), as observed also at Kurortne (Fig. 2) and probably characteristic for southeastern Europe, including the Black Sea region (Obreht et al., 2017).

The thickness of the Bug loess (ie., L1LL1) at Kurortne is much less compare to profiles up to 8–12 m reported in northern Ukraine (Gerasimenko, 2006; Rousseau et al., 2011; Bokhorst et al., 2011). Nevertheless, already in central Ukraine, the thickness of Bug unit on plateaus diminishes to 0.5–3 m, and in southeastern Ukraine, it does not exceed 1.5 m (Veklitch, 1993; Gerasimenko, 2004, 2011; Buggle et al., 2008, 2009).

In the Ukrainian Quaternary stratigraphical framework (Veklitch, 1993), the interval before the onset of the Holocene soil at 11.7 ka is related to the Prychornomorya loess unit, and in loess records from southeastern Ukraine, formation of incipient soils (the middle Prychornomorya subunit) was dated to this time interval (Gerasimenko, 2004, 2011). At Kurortne, χ results allow to place the end of the pleniglacial loess deposition and the onset of pedogenic processes that finally led to the formation of the Holocene soil already at around 13.8 ± 1.0 ka.

Furthermore, the identified succession of climatic events at Kurortne can be correlated with other similar LGC loess records in southeastern Europe (e.g. Mircea Vodă, Costinesti, Koriten and Semlac sections) (Constantin et al., 2014; Necula et al., 2013, 2015; Timar-Gabor et al., 2011; Jordanova and Petersen, 1999; Zeeden et al., 2016), and with the astronomically tuned χ record from the Titel/Stari Slankamen composite record from Serbia on its own age scale (Basarin et al., 2014). Fig. 6 shows the correlation of the Kurortne section based on χ as function of depth to loess sites from the Middle and Lower Danube Basin. This correlation is then compared to the benthic oxygen isotope stack (MIS 1 to MIS 6; Lisiecki and Raymo, 2005). All records show similar (climato)stratigraphic characteristics that, however, are temporarily better resolved in the thicker sequences (ie., Mircea Vodă, Koriten, Titel). Nevertheless, also the condensed sections with thicknesses of less than 5 m reveal an interesting pattern of relatively thick paleosol horizons compared to the loess intervals. These paleosol horizons even show typical stratigraphic susceptibility patterns easily recognizable across the Danube loess-paleosol sequences covering the LGC (Marković et al., 2015).

5. Conclusions

Following a multiproxy sedimentological and chronological investigation we show that for the uppermost 4.5 m of the loess-paleosol sequence exposed at Kurortne, the lowermost loess unit dated here prior to 123 ± 10 ka and corresponding to the Dnipro unit (equivalent to L2LL1; Marković et al., 2015) was succeeded by the formation of a thick interglacial-type chernozem paleosol, OSL dated in its upper part to 85.0 ± 6 ka (the Kaydaky unit, corresponding to S1SS2). Previous research corroborated by our observations indicate that this fossil chernozem belongs to the same subtype 'common chernozem' as the modern topsoil, but the carbonates are leached deeper, likely indicating wetter conditions during last interglacial than at present. The higher proportions of < 2 μm grain-size fraction in this paleosol also hints at more intense chemical weathering than during the Holocene and, thus, presumably milder climate during the emplacement of Kaydaky paleosol.

The Pryluky paleosol (corresponding to S1SS1), overlain by the Uday loess unit which is dated here to 61.2 ± 3.9 ka, is strongly enriched in carbonates, depleted in humus, with lower magnetic susceptibility values and a less abundant < 2 μm grain-size fraction than in the Kaydaky paleosol. These data support previously reported observations that the paleosol(s) comprised within the Pryluky unit most likely correspond to interstadial events of the early glacial (with lower chemical weathering indices than the underlying interglacial soil), and the whole Kaydaky-Pryluky sequence is correlative of MIS 5.

The Vytachiv paleosol (i.e., L1SS1) is positioned between the Uday loess (L1LL2, dated here to 61.2 ± 3.9 ka and thus corresponding to MIS 4) and the Bug loess (L1LL1, dated here to 25.8 ± 1.7 ka, and thus pertaining to the upper pleniglacial MIS 2) both characterized by low magnetic susceptibility values denoting loess accumulation under stadial conditions. The Vytachiv paleosol, OSL dated towards the top to 37.7 ± 2.4 ka is represented by a calcaric cambisol with magnetic susceptibility values and proportions of < 2 μm particles slightly higher than in the loess. These facts, as well as morphological features indicate that it represents an interstadial(s) formed during the middle pleniglacial (MIS 3). The observed increase in magnetic susceptibility and in the grain-size fraction < 2 μm in the lower part of the Vytachiv unit has also been reported in the other Ukrainian LPS.

The Late Pleistocene Prychornomorya loess unit dated at Kurortne between 13.8 ± 3.9 ka and 11.7 ± 0.8 ka (the Late Glacial, the last part of MIS 2) is represented by the carbonate horizon of the Holocene soil. The threshold in magnetic susceptibility values at the bottom of this unit marks the transition from the proper pleniglacial loess accumulation to the onset of pedogenic processes roughly around 20 ka. The intense pedogenesis during the Holocene interglacial resulted in the formation of a chernozem soil subtype 'common', which is typical S0 soil in the studied region of Ukraine.

The results discussed here based on integrating luminescence dating with multi-proxy sedimentological data for Kurortne LPS unequivocally ascertain to the LGC the uppermost 4.5 m of the section comprising the interval between first major paleosol (i.e., Kaydaky unit) and the Holocene S0 topsoil. This correlation fully supported by the OSL data helps in clarifying local chronostratigraphic correlations, establish more secure reconstructions of Late Pleistocene environmental changes in the northern Black Sea area, and test the correspondence with the Danube loess chronostratigraphic framework as discussed in Marković et al. (2015).

Acknowledgements

This research has received funding from the European Research Council (ERC) under the European Union's Horizon 2020 Research and Innovation Programme ERC-2015-STG (grant agreement No [678106]). F. Lehmkuhl and P. Schulte carried grain-size investigations in the context of the CRC 806 "Our way to Europe" funded by the Deutsche Forschungsgemeinschaft (DFG, German Research Foundation) – Projektnummer 57444011 – SFB 806. We thank Szabolcs Kelemen for gamma spectrometry measurements and Dr. Laura del Valle Villalonga for drawing the stratigraphic column. Comments and suggestions by two anonymous reviewers that helped improve the manuscript are gratefully acknowledged.

Appendix A. Supplementary data

Supplementary data to this article can be found online at https://doi.org/10.1016/j.quaint.2020.03.001.

References

Adamiec, G., Aitken, M.J., 1998. Dose-rate conversion factors: update. Ancient TL 16, 37–50.

Aitchison, J., 1986. The Statistical Analysis of Compositional Data. Chapman and Hall, London, UK. https://doi.org/10.1007/978-94-009-4109-0.

Aitken, M.J., 1976. Thermoluminescent age evaluation and assessment of error limits: revised system. Archaeometry 18, 233–238. https://doi.org/10.1111/j.1475-4754.1976.tb00168.x.

Aitken, M.J., 1985. Thermoluminescence Dating. Academic Press, London, pp. 153.

Aitken, M.J., Alldred, J.C., 1972. The assessment of error limits in thermoluminescent dating. Archaeometry 14, 257–267. https://doi.org/10.1111/j.1475-4754.1972.tb00068.x.

Anderson, R.S., Hallet, B., 1996. Simulating magnetic susceptibility profiles in loess as an aid in quantifying rates of dust deposition and pedogenic development. Quat. Res. 45, 1–16. https://doi.org/10.1006/qres.1996.0001.

Anechitei-Deacu, V., Timar-Gabor, A., Fitzsimmons, K.E., Veres, D., Hambach, U., 2014. Multi-method luminescence investigations on quartz grains of different sizes extracted from a loess section in southeast Romania interbedding the Campanian Ignimbrite ash layer. Geochronometria 41, 1–14. https://doi.org/10.2478/s13386-013-0143-4.

Bakhmutov, V.G., Kazansky, A.Y., Matasova, G.G., Glavatskii, D.V., 2017. Petromagnetism and magnetostratigraphy of Ukrainian loess/palaeosol sequence (Roxolany, Boyanichi and Korshev sections). Izvestiya Phys. Solid Earth (Fizika Zemli) 53, 864–884.

Basarin, B., Buggle, B., Hambach, U., Marković, S.B., Dhand, K.O., Kovačević, A., Stevens, T., Guo, Z., Lukić, T., 2014. Time-scale and astronomical forcing of Serbian loess–paleosolsequences. Global Planet. Change 122, 89–106. https://doi.org/10.1016/j.gloplacha.2014.08.007.

Blott, S.J., Pye, K., 2006. Particle size distribution analysis of sand-sized particles by laser diffraction: an experimental investigation of instrument sensitivity and the effects of particle shape: particle size distribution analysis of sands by laser diffraction. Sedimentology 53, 671–685. https://doi.org/10.1111/j.1365-3091.2006.00786.x.

Boguckyj, A., Lanczont, M., 2002. Loess stratigraphy in the Halyc Prydnistrov'ja region. Stud. Geol. Pol. 119, 366–374.

Boguckyj, A., Gozhik, P., Lanczont, M., Madeyska, T., Jelowiczowa, Ja (Eds.), 2013. Lesovyj Pokryv Pivnichnogo Prychornomorya (Loess Cover of the Northern Black Sea Shore). Kartrol, Lublin (in Ukrainian and Polish).

Bokhorst, M., Vandenberge, J., Sumegi, P., Lanzont, M., Gerasimenko, N., Matviishina, Zh, Markovich, S., Frechen, M., 2011. Atmospheric circulation patterns in central and eastern Europe during the Weichselian pleniglacial inferred from loess grain-size record. Quat. Int. 1–2, 62–74. https://doi.org/10.1016/j.quaint.2010.07.018.

Bolikhovskaya, N.S., Molodkov, A.N., 2006. East European loess-palaeosol sequence: palynology, stratigraphy and correlation. Quat. Int. 149, 24–36. https://doi.org/10.1016/j.quaint.2005.11.015.

Buggle, B., Glaser, B., Zöller, L., Hambach, U., Marković, S., Glaser, I., Gerasimenko, N., 2008. Geochemical characterization and origin of Southeastern and Eastern European loesses (Serbia, Romania, Ukraine). Quat. Sci. Rev. 27, 1058–1075. https://doi.org/10.1016/j.quascirev.2008.01.018.

Buggle, B., Hambach, U., Glaser, B., Gerasimenko, N., Marković, S., Glaser, I., Zöller, L., 2009. Stratigraphy, and spatial and temporal paleoclimatic trends in Southeastern/Eastern European loess–paleosol sequences. Quat. Int. 196, 86–106. https://doi.org/10.1016/j.quaint.2008.07.013.

Buggle, B., Hambach, U., Müller, K., Zöller, L., Marković, S.B., Glaser, B., 2014. Iron mineralogical proxies and Quaternary climate change in SE-European loess–paleosol sequences. Catena 117, 4–22. https://doi.org/10.1016/j.catena.2013.06.012.

Buurman, P., Pape, T., Muggler, C.C., 1997. Laser grain-size determination in soil genetic studies. 1. Practical problems. Soil Sci. 162 (3), 211–218.

Buylaert, J.P., Murray, A.S., Huot, S., Vriend, M.G.A., Vandenberghe, D., De Corte, F., Van den haute, P., 2006. A comparison of quartz OSL and isothermal TL measurements on Chinese loess. Radiat. Protect. Dosim. 119, 474–478. https://doi.org/10.1093/rpd/nci518.

Chabai, V.P., Monigal, K. (Eds.), 1999. Middle Paleolithic of Western Crimea, vol. 2 ERAUL, Liege 87.

Constantin, D., Timar-Gabor, A., Veres, D., Begy, R., Cosma, C., 2012. SAR-OSL dating of different grain-sized quartz from a sedimentary section in southern Romania interbedding the Campanian Ignimbrite/Y5 ash layer. Quat. Geochronol. 10, 81–86. https://doi.org/10.1016/j.quageo.2012.01.012.

Constantin, D., Begy, R., Vasiliniuc, S., Panaiotu, C., Necula, C., Codrea, V., Timar-Gabor, A., 2014. High-resolution OSL dating of the Costinesti section (Dobrogea, SE Romania) using fine and coarse quarz. Quat. Int. 334–335, 20–29. https://doi.org/10.1016/j.quaint.2013.06.016.

Constantin, D., Veres, D., Panaiotu, C., Anechitei-Deacu, V., Groza, S.M., Begy, R., Kelemen, S., Buylaert, J.-P., Hambach, U., Marković, S.B., Gerasimenko, N., Timar-Gabor, A., 2019. Luminescence age constraints on the Pleistocene-Holocene transition recorded in loess sequences across SE Europe. Quat. Geochronol. 49, 71–77. https://doi.org/10.1016/j.quageo.2018.07.011.

Cunningham, A.C., Wallinga, J., 2010. Selection of integration time intervals for quartz OSL decay curves. Quat. Geochronol. 5, 657–666. https://doi.org/10.1016/j.quageo.2010.08.004.

Dodonov, A.E., Zhou, L.P., Markova, A.K., Tchepalyga, A.L., Trubikhin, V.M., Akesandrovski, A.L., Simakova, A.N., 2006. Middle-upper Pleistocene bio-climatic and magnetic records of the northern Black Sea Coastal area. Quat. Int. 149, 44–54. https://doi.org/10.1016/j.quaint.2005.11.017.

Duller, G.A.T., 2003. Distinguishing quartz and feldspar in single grain luminescence measurements. Radiat. Meas. 37, 161–165. https://doi.org/10.1016/S1350-4487(02)00170-1.

Fitzsimmons, K.E., 2017. Reconstructing palaeoenvironments on desert margins: new perspectives from Eurasian loess and Australian dry lake shorelines. Quat. Sci. Rev. 171, 1–19. https://doi.org/10.1016/j.quascirev.2017.05.018.

Forster, T., Evans, M.E., Heller, F., 1994. The frequency dependence of low field susceptibility in loess sediments. Geophys. J. Int. 118 (3), 636–642. https://doi.org/10.1111/j.1365-246X.1994.tb03990.x.

Frechen, M., Oches, E.A., Kohfeld, K.E., 2003. Loess in Europe - mass accumulation rates during the last glacial period. Quat. Sci. Rev. 22, 1835–1857. http://hdl.handle.net/11858/00-001M-0000-000E-D03F-0.

Gendler, T.S., Heller, F., Tsatskin, A., Spassov, S., Du Pasquier, J., Faustov, S.S., 2006. Roxolany and Novaya Etuliya - key sections in the western Black Sea loess area: magnetostratigraphy, rock magnetism, and paleopedology. Quat. Int. 152–153, 78–93. https://doi.org/10.1016/j.quaint.2006.01.001.

Gerasimenko, N., 1999. Late Pleistocene vegetational history of Kabazi II. The middle paleolithic of western Crimea. ERAUL 2, 115–141 87.

Gerasimenko, N.P., 2004. Rozvytok Zonal'nyh Landshaftiv Chetvertynnogo Periodu V Ukraina (Quaternary Evolution of Zonal Paleoecosystems in Ukraine). Geographical Institute of National Ukrainian Academy of Sciences, Kyiv (in Ukrainian).

Gerasimenko, N., 2006. Upper Pleistocene loess-palaeosol and vegetational successions in the middle Dnieper area, Ukraine. Quat. Int. 149, 55–66. https://doi.org/10.1016/j.quaint.2005.11.018.

Gerasimenko, N., 2010. The Late Pleistocene environmental changes from the northern Ukraine to the southern Crimea as evidenced by pollen. 2010 annual meeting INQUA-SEQS, Rostov-on-Don, Russia, June 21-26, 2010. In: Titov, V.V., Tesakov, A.S. (Eds.), Quaternary Stratigraphy and Paleontology of the Southern Russia: Connections between Europe, Africa and Asia, pp. 24–27.

Gerasimenko, N., 2011. Climatic and environmental oscillations in southeastern Ukraine from 30 to 10 ka, inferred from pollen and lithopedology. Geology and geoarchaeology of the Black Sea region: beyond the Flood hypothesis. Geol. Soc. Am. Spec. Pap. 473, 117–132. https://doi.org/10.1130/2011.2473(08.

Gozhik, P., 2013. Study Questions of Roxolany Section. Loess-Covering of the North Black Sea Region. Lublin. KARTPOL s.c, Lublin, pp. 17–33 (in Ukrainian).

Gozhik, P., Shelkoplyas, V., Khristoforova, T., 1995. Development stages of loessial and glacial formations in Ukraine. Annales UMCS, Sec. B 50, 65–74.

Gozhik, P.F., Shelkoplyas, V.M., Komar, M.S., Matviishina, ZhM., Perederiy, V.I., 2000. Putivnyk X Pol'sko-Ukrainskogo Seminaru „Koreluatsia Lesiv I Lyodovykovyh Vidkladiv Pol'shchi Ta Ukrainy (Excursion Guide of Xth Polish-Ukrainian Seminar "Correlation of Loesses and Glacial Deposits of Poland and Ukraine"). Institute of Geological Sciences, Kyiv.

Gozhik, P., Matviishina, Zh, Shelkoplyas, V., Palienko, V., Rekovets, L., Gerasimenko, N., Korniets, N., 2001. The upper and middle Pleistocene of Ukraine. In: The Ukraine Quaternary Explored: the Middle and Upper Pleistocene of the Middle Dnieper Area and its Importance for the East-West Correlation, Volume of Abstracts. IGS NASU, Kyiv, pp. 32–34.

Gozhik, P., Komar, M., Lanćzont, M., Fedorovicz, S., Bogucki, A., Mroczek, P., Prylypko, S., Kusiak, J., 2014. Paleoenvironmental history of the middle Dnieper area from the Dnieper to Weichselian Glaciation: a case study of the Maxymivka loess profile. Quat. Int. 334–335, 94–111. https://doi.org/10.1016/j.quaint.2013.11.037.

Gożik, P.F., Czugunnyj, V., Mielnik, V., et al., 1976. Guide to VIII Intern. Symp. On Loessial Rocks. Inst. Geol. Nauk Akad. Nauk USSR, Kiev.

Haase, D., Fink, J., Haase, G., Ruske, R., Pécsi, M., Richter, H., Altermann, M., Jäger, K.-D., 2007. Loess in Europe - its spatial distribution based on a European loess map, 1:2500000. Quat. Sci. Rev. 26, 1301–1312. https://doi.org/10.1016/j.quascirev.2007.02.003.

Haesaerts, P., Damblon, F., Gerasimenko, N., Spagna, P., Pirson, S., 2016. The Late Pleistocene loess-palaeosol sequence of Middle Belgium. Quat. Int. 411, 25–43. https://doi.org/10.1016/j.quaint.2016.02.012.

Hansen, V., Murray, A., Buylaert, J.-P., Yeo, E.-Y., Thomsen, K., 2015. A new irradiated quartz for beta source calibration. Radiat. Meas. 81, 123–127. https://doi.org/10.1016/j.radmeas.2015.02.017.

Hao, Q.Z., Wang, L., Oldfield, F., Peng, S.Z., Qin, L., Song, Y., Xu, B., Qiao, Y., Bloemendal, J., Guo, Z.T., 2012. Delayed build-up of Arctic ice sheets during 400,000-year minima in insolation variability. Nature 490, 393–396. https://doi.org/10.1038/nature11493.

Haynes, W.M. (Ed.), 2015. CRC Handbook of Chemistry and Physics, 96th Edition, 96 edition. CRC Press, Boca Raton, Florida.

ISO 11277, 2002. Soil Quality - Determination of Particle Size Distribution in Mineral Soil Material - Method by Sieving and Sedimentation. International Organization for Standardization, Geneva.

ISO 13320, 2009. Particle Size Analysis - Laser Diffraction Methods. International Organization for Standardization, Geneva.

Jordanova, D., Petersen, N., 1999. Palaeoclimatic record from a loess-soil profile in northeastern Bulgaria—II. Correlation with global climatic events during the Pleistocene. Geophys. J. Int. 138 (2), 533–540. https://doi.org/10.1046/j.1365-246X.1999.00873.x.

Kadereit, A., Wagner, G., 2014. Geochronological reconsideration of the eastern European key loess section at Stayky in Ukraine. Clim. Past 10, 783–796. https://doi.org/10.5194/cp-10-783-2014.

Krypskyi, N.K., Polupan, N.I., 1979. Atlat Pochv Ukrainskoy SSR (Soil Atlas of the Ukrainian SSR). Urozhay, Kiev (in Ukrainian).
Kusiak, J., 2007. True and anomalous TL dates from late Pleistocene loess-palaeosol deposits at the Kolodiiv site (east Carpathian Foreland, Ukraine). Geol. Q. 51, 167–172. https://gq.pgi.gov.pl/article/view/7445.
Łanczont, M., Bogucki, A.B., Kusiak, J., Sytnyk, O., 2013. The results of thermo-luminescence dating in the Halych IIC (Ukraine) profile as the expression of the conditions of mineral material deposition. Geochronometria 40 (1), 42–50. https://doi.org/10.2478/s13386-012-0022-4.
Lagasse, R.R., Richards, D.W., 2003. Determining the size distribution of core–shell spheres and other complex particles by laser diffraction. J. Colloid Interface Sci. 267, 65–73. https://doi.org/10.1016/S0021-9797(03)00669-6.
Lai, Z.P., Murray, A.S., Bailey, R.M., Huot, S., Bøtter-Jensen, L., 2006. Quartz red TL SAR equivalent dose overestimation for Chinese loess. Radiat. Meas. 41, 114–119. https://doi.org/10.1016/j.radmeas.2005.06.006.
Lapp, T., Kook, M., Murray, A.S., Thomsen, K.J., Buylaert, J.-P., Jain, M., 2015. A new luminescence detection and stimulation head for the Risø TL/OSL reader. Radiat. Meas. 81, 178–184. https://doi.org/10.1016/j.radmeas.2015.02.001.
Lindner, L., Gozhik, P., Marciniak, B., Marks, L., Yelovicheva, Y., 2004. Main climatic changes in the Quaternary of Poland, Belarus and Ukraine. Geol. Q. 48 (2), 97–114. https://gq.pgi.gov.pl/article/view/7336.
Lindner, L., Bogucki, A., Gozhik, P., Marks, L., Lanćzont, M., Wojtanovicz, J., 2006. Correlation of the Pleistocene deposits in the area between the Baltic and Black Sea, central Europe. Geol. Q. 50, 195–210. https://gq.pgi.gov.pl/article/view/7405.
Lisiecki, L.E., Raymo, M.E., 2005. A Pliocene-Pleistocene stack of 57 globally distributed benthic $\delta^{18}O$ records. Paleoceanography 20, PA1003. https://doi.org/10.1029/2004PA001071.
Maher, B.A., 2011. The magnetic properties of Quaternary aeolian dusts and sediments, and their palaeoclimatic significance. Aeolian Res. 3, 87–144. https://doi.org/10.1016/j.aeolia.2011.01.005.
Maher, B.A., Prospero, J.M., Mackie, D., Gaiero, D., Hesse, P.P., Balkanski, Y., 2010. Global connections between aeolian dust, climate and ocean biogeochemistry at the present day and at the last glacial maximum. Earth Sci. Rev. 99 (1–2), 61–97. https://doi.org/10.1016/j.earscirev.2009.12.001.
Marković, S.B., Stevens, T., Kukla, G.J., Hambach, U., Fitzsimmons, K.E., Gibbard, P., Buggle, B., Zech, M., Guo, Z., Hao, Q., Wu, H., O'Hara Dhand, K., Smalley, I.J., Újvári, G., Sümegi, P., Timar-Gabor, A., Veres, D., Sirocko, F., Vasiljević, D.A., Jary, Z., Svensson, A., Jović, V., Lehmkuhl, F., Kovács, J., Svirčev, Z., 2015. Danube loess stratigraphy —towards a pan-European loess stratigraphic model. Earth Sci. Rev. 148, 228–258. https://doi.org/10.1016/j.earscirev.2015.06.005.
Marković, S.B., Stevens, T., Mason, J., Vandenberghe, J., Yang, S., Veres, D., Újvári, G., Timar-Gabor, A., Zeeden, C., Goš, Z., Hao, Q., Obreht, I., Hambach, U., Wu, H., Gavrilov, M.B., Rolf, C., Tomić, N., Lehmkuhl, F., 2018. Loess correlations–Between myth and reality. Palaeogeogr. Palaeoclimatol. Palaeoecol. 509, 4–23. https://doi.org/10.1016/j.palaeo.2018.04.018.
Matviishina, ZhM., Gerasimenko, N.P., Perederiy, V.I., Ivchenko, A.S., Karmazinenko, S.P., Parkhomenko, O.G., 2010. Prostorovo-chasova Korelyatsia Paleogeografichnyh Umov Chetvertynnogo Periodu Na Territorii Ukrainy (Spatial-Temporal Correlation of the Palaeogeographical Events during the Quaternary in Ukraine). Nauka, Kyiv, pp. 2010 (in Ukrainian).
McCave, I.N., Syvitski, J.P.M., 1991. Principles and methods of geological particle size analysis. In: Syvitski, J.P.M. (Ed.), Principles, Methods, and Application of Particle Size Analysis. Cambridge University Press, pp. 129–142.
Mejdahl, V., 1979. Thermoluminescence dating: beta-dose attenuation in quartz grains. Archaeometry 21, 61–72. https://doi.org/10.1111/j.1475-4754.1979.tb00241.x.
Mishchenko, M.I., 1993. Light scattering by size–shape distributions of randomly oriented axially symmetric particles of a size comparable to a wavelength. Appl. Optic. 32, 4652–4666.
Moine, O., Antoine, P., Hatté, C., Landais, A., Mathieu, J., Prud'homme, C., Rousseau, D.-D., 2017. The impact of Last Glacial climate variability in west-European loess revealed by radiocarbon dating of fossil earthworm granules. Proc. Natl. Acad. Sci. Unit. States Am. 114, 6209–6214. https://doi.org/10.1073/pnas.1614751114.
Murray, A.S., Wintle, A.G., 2000. Luminescence dating of quartz using an improved single-aliquot regenerative-dose protocol. Radiat. Meas. 32, 57–73. https://doi.org/10.1016/S1350-4487(99)00253-X.
Murray, A.S., Wintle, A.G., 2003. The single aliquot regenerative dose protocol: potential for improvements in reliability. Radiat. Meas. 37, 377–381. https://doi.org/10.1016/S1350-4487(03)00053-2.
Nawrocki, J., Bakhmutov, V., Bogucki, A., Dolecki, L., 1999. The paleo- and petromagnetic record in the Polish and Ukrainian loess-palaeosol sequences. Phys. Chem. Earth (A) 24 (9), 773–777. https://doi.org/10.1016/S1464-1895(99)00113-1.
Nawrocki, J., Gozhik, P., Łanczont, M., Pańczyk, M., Komar, M., Bogucki, A., Williams, I.S., Czupyt, Z., 2018. Palaeowind directions and sources of detrital material archived in the Roxolany loess section (southern Ukraine). Palaeogeogr. Palaeoclimatol. Palaeoecol. 496, 121–135. https://doi.org/10.1016/j.palaeo.2018.01.028.
Necula, C., Panaiotu, C., Heslop, D., Dimofte, D., 2013. Climatic control of magnetic granulometry in the Mircea Vodă loess/paleosol sequence (Dobrogea, Romania). Quat. Int. 293, 5–14. https://doi.org/10.1016/j.quaint.2012.03.043.
Necula, C., Dimofte, D., Panaiotu, C., 2015. Rock magnetism of a loess-palaeosol sequence from the western Black Sea shore (Romania). Geophys. J. Int. 202 (3), 1733–1748. https://doi.org/10.1093/gji/ggv250.
Nesbitt, H.W., Young, G.M., 1982. Early Proterozoic climates and plate motions inferred from major element chemistry of lutites. Nature 299, 715–717. https://doi.org/10.1038/299715a0.
Obreht, I., Hambach, U., Veres, D., Zeeden, C., Bösken, J., Stevens, T., Marković, S.B., Klasen, N., Brill, D., Burow, C., Lehmkuhl, F., 2017. Shift of large-scale atmospheric systems over Europe during late MIS 3 and implications for Modern Human dispersal. Sci. Rep. 7, 5848. https://doi.org/10.1038/s41598-017-06285-x.
Obreht, I., Zeeden, C., Hambach, U., Veres, D., Marković, S.B., Lehmkuhl, F., 2019. A critical reevaluation of palaeoclimate proxy records from loess in the Carpathian Basin. Earth Sci. Rev. 190, 498–520. https://doi.org/10.1016/j.earscirev.2019.01.020.
Özer, M., Orhan, M., Işik, N.S., 2010. Effect of particle optical properties on size distribution of soils obtained by laser diffraction. Environ. Eng. Geosci. 16, 163–173. https://doi.org/10.2113/gseegeosci.16.2.163.
Perić, Z., Lagerbäck Adolphi, E., Stevens, T., Újvári, G., Zeeden, C., Buylaert, J.-P., Marković, S.B., Hambach, U., Fischer, P., Schmidt, C., Schulte, P., Huayu, L., Shuangwen, Y., Lehmkuhl, F., Obreht, I., Veres, D., Thiel, C., Frechen, M., Jain, M., Vött, A., Zöller, L., Gavrilov, M.B., 2019. Quartz OSL dating of late quaternary Chinese and Serbian loess: a cross Eurasian comparison of dust mass accumulation rates. Quat. Int. 502 (Part A), 30–44. https://doi.org/10.1016/j.quaint.2018.01.010.
Poznyak, S.P., 2010. Gruntoznavstvo I Geografia Gruntiv (Soil Science and Geography of Soils). LNU imeni Ivana Franka, L'viv (in Ukrainian).
Prescott, J.R., Hutton, J.T., 1994. Cosmic ray contributions to dose rates for luminescence and ESR dating: large depths and long term variations. Radiat. Meas. 23, 497–500. https://doi.org/10.1016/1350-4487(94)90086-8.
Qiang, M., Lang, L., Wang, Z., 2010. Do fine-grained components of loess indicate westerlies: insights from observations of dust storm deposits at Lenghu (Qaidam Basin, China). J. Arid Environ. 74, 1232–1239. https://doi.org/10.1016/j.jaridenv.2010.06.002.
Radaković, M.G., Gavrilov, M.B., Hambach, U., Schaetzl, R.J., Tošić, I., Ninkov, J., Vasin, J., Marković, S.B., 2019. Quantitative relationships between climate and magnetic susceptibility of soils on the Bačka Loess Plateau (Vojvodina, Serbia). Quat. Int. 502, 85–94. https://doi.org/10.1016/j.quaint.2018.04.040.
Rasmussen, S.O., Bigler, M., Blockley, S.P., Blunier, T., Buchardt, S.L., Clausen, H.B., Cvijanovic, I., Dahl-Jensen, D., Johnsen, S.J., Fischer, H., Gkinis, V., Guillevic, M., Hoek, W.Z., Lowe, J.J., Pedro, J.B., Popp, T., Seierstad, I.K., Steffensen, J.P., Svensson, A.M., Vallelonga, P., Vinther, B.M., Walker, M.J.C., Wheatley, J.J., Winstrup, M., 2014. A stratigraphic framework for abrupt climatic changes during the Last Glacial period based on three synchronized Greenland ice-core records: refining and extending the INTIMATE event stratigraphy. Quat. Sci. Rev. 106, 14–28. https://doi.org/10.1016/1350-4487(94)90086-8.
Rees-Jones, J., 1995. Optical dating of young sediments using fine-grain quartz. Ancient TL 13, 9–13.
Rousseau, D.-D., Gerasimenko, N., Matviishina, Zh, Kukla, G., 2001. Late Pleistocene environments of Central Ukraine. Quat. Res. 56, 349–356. https://doi.org/10.1006/qres.2001.2270.
Rousseau, D.-D., Antoine, P., Gerasimenko, N., Sima, A., Fuchs, M., Hatté, C., Moine, O., Zoeller, L., 2011. North Atlantic abrupt climatic events of the last glacial period recorded in Ukrainian loess deposits. Clim. Past 7, 221–234. https://doi.org/10.5194/cp-7-221-2011.
Rousseau, D.-D., Boers, N., Sima, A., Svensson, A., Bigler, M., Lagroix, F., Taylor, S., Antoine, P., 2017. (MIS3 & 2) millennial oscillations in Greenland dust and Eurasian aeolian records – a paleosol perspective. Quat. Sci. Rev. 169, 99–113. https://doi.org/10.1016/j.quascirev.2017.05.020.
Schaetzl, R., Bettis, E.A., Crouvi, O., Fitzsimmons, K.E., Grimley, D.A., Hambach, U., Lehmkuhl, F., Marković, S.B., Mason, J.A., Owczarek, P., Roberts, H.M., Rousseau, D.-D., Stevens, T., Vandenberghe, J., Zárate, M., Veres, D., Yang, S., Zech, M., Conroy, J.L., Dave, A.K., Faust, D., Hao, Q., Obreht, I., Prud'homme, C., Smalley, I., Tripaldi, A., Zeeden, C., Zech, R., 2018. Approaches and challenges to the study of loess - introduction to the Loess Fest special issue. Quat. Res. 89, 563–618. https://doi.org/10.1017/qua.2018.15.
Schulte, P., Lehmkuhl, F., 2018. The difference of two laser diffraction patterns as an indicator for post-depositional grain size reduction in loess-paleosol sequences. Palaeogeogr. Palaeoclimatol. Palaeoecol. 509, 126–136. https://doi.org/10.1016/j.palaeo.2017.02.022.
Schulte, P., Lehmkuhl, F., Steininger, F., Loibl, D., Lockot, G., Protze, J., Fischer, P., Stauch, G., 2016. Influence of HCl pretreatment and organo-mineral complexes on laser diffraction measurement of loess–paleosol-sequences. Catena 137, 392–405. https://doi.org/10.1016/j.catena.2015.10.015.
Sirenko, N.A., Turlo, S.I., 1986. Razvitie Pochv I Rastitel'nosti Ukrainy V Pliotsene I Pleistostene (Soil and Vegetational Development in Ukraine during the Pliocene and Pleistocene). Naukova Dumka, Kyiv (in Russian).
Spectro, 2007. Analysis of Trace Elements in Geological Materials, Soils and Sludges Prepared as Pressed Pellets, Report XRF. SPECTRO.
Stevens, T., Buylaert, J.-P., Thiel, C., Újvári, G., Yi, S., Murray, A.S., Frechen, M., Lu, H., 2018. Ice-volume-forced erosion of the Chinese Loess Plateau global Quaternary stratotype site. Nat. Commun. 9, 983. https://doi.org/10.1038/s41467-018-03329-2.
Sümegi, P., Gulyás, S., Molnár, D., Sümegi, B.P., Törőcsik, T., Almond, P.C., Koloszár, L., 2019. Periodicities of paleoclimate variations in the first high-resolution non-orbitally tuned grain size record of the past 1 Ma from SW Hungary and regional, global correlations. Aeolian Res. 40, 74–90. https://doi.org/10.1016/j.aeolia.2019.07.002.
Thomsen, K.J., Bøtter-Jensen, L., Denby, P.M., Moska, P., Murray, A.S., 2006. Developments in luminescence measurement techniques. Radiat. Meas. 41, 768–773. https://doi.org/10.1016/j.radmeas.2006.06.010.
Timar, A., Vandenberghe, D., Panaiotu, C.G., Necula, C., Cosma, C., van den Haute, P., 2010. Optical dating of Romanian loess using fine-grained quartz. Quat. Geochronol. 5, 143–148. https://doi.org/10.1016/j.quageo.2009.03.003.
Timar-Gabor, A., Vandenberghe, D.A.G., Vasiliniuc, S., Panaiotu, C.G., Dimofte, D., Cosma, C., 2011. Optical dating of Romanian loess: a comparison between silt-sized and sand-sized quartz. Quat. Int. 240, 62–70. https://doi.org/10.1016/j.quaint.2010.10.007.

Timar-Gabor, A., Vasiliniuc, S., Vandenberghe, D.A.G., Cosma, C., Wintle, A.G., 2012. Investigations into the reliability of SAR-OSL equivalent doses obtained for quartz samples displaying dose response curves with more than one component. Radiat. Meas. 47, 740–745. https://doi.org/10.1016/j.radmeas.2011.12.001.

Timar-Gabor, A., Constantin, D., Marković, S.B., Jain, M., 2015. Extending the area of investigation of fine versus coarse quartz optical ages from the Lower Danube to the Carpathian Basin. Quat. Int. 388, 168–176. https://doi.org/10.1016/j.quaint.2014.09.065.

Timar-Gabor, A., Buylaert, J.-P., Guralnik, B., Trandafir-Antohi, O., Constantin, D., Anechitei-Deacu, V., Jain, M., Murray, A.S., Porat, N., Hao, Q., Wintle, A.G., 2017. On the importance of grain size in luminescence dating using quartz. Radiat. Meas. 106, 464–471. https://doi.org/10.1016/j.radmeas.2017.01.009.

Tsatskin, A., Heller, F., Hailwood, E.A., Gendler, T.S., Hus, J., Montgomery, P., Sartori, M., Virina, E.I., 1998. Pedosedimentary division, rock magnetism and chronology of the loess/palaeosol sequence at Roxolany (Ukraine). Palaeogeogr. Palaeoclimatol. Palaeoecol. 143, 111–133. https://doi.org/10.1016/S0031-0182(98)00073-X.

Újvári, G., Kok, J.F., Varga, G., Kovács, J., 2016. The physics of wind-blown loess: implications for grain size proxy interpretations in Quaternary paleoclimate studies. Earth Sci. Rev. 154, 247–278. https://doi.org/10.1016/j.earscirev.2016.01.006.

Újvári, G., Stevens, T., Molnár, M., Demény, A., Lambert, F., Varga, G., Jull, A.J.T., Páll-Gergely, B., Buylaert, J.-P., Kovács, J., 2017. Coupled European and Greenland last glacial dust activity driven by North Atlantic climate. Proc. Natl. Acad. Sci. Unit. States Am. 114, E10632. http://www.pnas.org/content/114/50/E10632.abstract.

Újvári, G., Wegner, W., Klötzli, U., Horschinegg, M., Hippler, D., 2018. Sr-Nd-Hf isotopic analysis of < 10 mg dust samples: implications for ice core dust source fingerprinting. G-cubed 19 (1), 60–72. https://doi.org/10.1002/2017GC007136.

Vandenberghe, D.A.G., De Corte, F., Buylaert, J.-P., Kucera, J., Van den haute, P., 2008. On the internal radioactivity in quartz. Radiat. Meas. 43, 771–775. https://doi.org/10.1016/j.radmeas.2008.01.016.

Vasiliniuc, S., Timar-Gabor, A., Vandenberghe, D.A.G., Panaiotu, C.G., Begy, R.C., Cosma, C., 2011. A high resolution optical dating study of the Mostiștea loess-palaeosol sequence (SE Romania) using sand-sized quartz. Geochronometria 38, 34–41. https://doi.org/10.2478/s13386-011-0007-8.

Veklitch, M.F., 1982. "Paleoetapnost' I Stratotipy Pochvennyh Formatsiy Ukrainy" (Paleogeographical Stages and Stratotypes of Soil Formations of Ukraine). Naukova dumka, Kiev (In Russian).

Veklitch, M.F. (Ed.), 1993. Stratigraficheskya Shema Chetvertichnyh Otlozheniy Ukrainy (Stratigraphical Scheme of Quaternary Deposits of Ukraine). State Committee for Geology of Ukraine, Kyiv (in Russian).

Veklitch, Yu M., 2018. Geoeolovyi Morfolitogenes Ta Metodologichni Aspekty Yogo Doslidzhennya (Geoeolian Morpholithogenesis and Methodological Aspects of its Study). UkrDGRI, Kyiv (in Ukrainain).

Veklitch, M.F., Artyushenko, A.T., Sirenko, N.A., Dubnyak, V.A., Mel'nichuk, I.V., Parishkura, S.I., 1967. Opornye Geologicheskie Razrezy Antropogena Ukrainy (Key Sites of the Ukrainian Quaternary), vol. 1 Naukova dumka, Kiev (in Russian).

Velichko, A.A., 1990. Loess-paleosol formation on the Russian plain. Quat. Int. 7/8, 103–114. https://doi.org/10.1016/1040-6182(90)90044-5.

Veres, D., Lane, C.S., Timar-Gabor, A., Hambach, U., Constantin, D., Szakács, A., Fülling, A., Onac, B.P., 2013. The Campanian Ignimbrite/Y5 tephra layer – a regional stratigraphic marker for Isotope Stage 3 deposits in the Lower Danube region, Romania. Quat. Int. 293, 22–33. https://doi.org/10.1016/j.quaint.2012.02.042.

Veres, D., Tecsa, V., Gerasimenko, N., Zeeden, C., Hambach, U., Timar-Gabor, A., 2018. Short-term soil formation events in last glacial East European loess, evidence from multi-method luminescence dating. Quat. Sci. Rev. 200, 34–51. https://doi.org/10.1016/j.quascirev.2018.09.037.

Vozgrin, B.D., 2001. Problemy stratygrafichnogo rozchlenuvannya ta korelyatsii kontynental'nyh vidkladiv antropogenu Ukrainy (Problems of stratigraphic subdivision and correlation of the Quaternary continental deposits in Ukraine). In: Regional'ni Geologichni Doslidzhennya v Ukraini i Pytannya Stvorennya Derzhgeolkarty – 2001. The State Geological Survey, Ukrainian State Research Institute for Geological Survey, Kyiv (in Ukrainian).

Vozgrin, B.D., 2005. Pro resul'taty doslidzhen' iz vdoskonalennya stratygrafichnoi shemy chetvertynnuh vidkladiv Ukrainy (On results of the studies on improvement of the Quaternary stratigraphical framework of Ukraine). In: Suchasnyi Stan i Zadachi Rozvytku Regional'nyh Geologichnyh Doslidzhen'. The State Geological Survey, Ukrainian State Research Institute for Geological Survey, Kyiv (in Ukrainian).

Wintle, A.G., Murray, A.S., 2006. A review of quartz optically stimulated luminescence characteristics and their relevance in single-aliquot regeneration dating protocols. Radiat. Meas. 41, 369–391. https://doi.org/10.1016/j.radmeas.2005.11.001.

Zeeden, C., Kels, H., Hambach, U., Schulte, P., Protze, J., Eckmeier, E., Marković, S.B., Klasen, N., Lehmkuhl, F., 2016. Three climatic cycles recorded in a loess-palaeosol sequence at Semlac (Romania) – implications for dust accumulation in south-eastern Europe. Quat. Sci. Rev. 154, 130–142. https://doi.org/10.1016/j.quascirev.2016.11.002.

Zeeden, C., Hambach, U., Obreht, I., Hao, Q., Abels, H.A., Veres, D., Lehmkuhl, F., Gavrilov, M.B., Marković, S.B., 2018a. Patterns and timing of loess-paleosol transitions in Eurasia: constraints for paleoclimate studies. Global Planet. Change 162, 1–7. https://doi.org/10.1016/j.gloplacha.2017.12.021.

Zeeden, C., Hambach, U., Veres, D., Fitzsimmons, K., Obreht, I., Bösken, J., Lehmkuhl, F., 2018b. Millennial scale climate oscillations recorded in the Lower Danube loess over the last glacial period. Palaeogeogr. Palaeoclimatol. Palaeoecol. 509, 164–181. https://doi.org/10.1016/j.palaeo.2016.12.029.

Zeeden, C., Obreht, I., Veres, D., Kaboth-Bahr, S., Hošek, J., Marković, S.B., Bösken, J., Lehmkuhl, F., Rolf, C., Hambach, U., 2020. Smoothed millennial-scale palaeoclimatic reference data as unconventional comparison targets: application to European loess records. Sci. Rep.